Solar Energy Materials & Solar Cells 272 (2024) 112900

Contents lists available at ScienceDirect

Solar Energy Materials and Solar Cells

journal homepage: www.elsevier.com/locate/solmat

Photochromism in rare earth oxyhydrides for large-area transmittance control☆

José Montero-Amenedo

Department of Materials Science and Engineering, Uppsala University, Lägerhyddsvägen 1, Uppsala, 75237, Sweden

ARTICLE INFO

Keywords:
Chromogenic materials
Oxyhydrides
Photochromism
Smart windows

ABSTRACT

Photochromic coatings are attractive materials for achieving dynamic transmittance control in glazing. However, state-of-the-art photochromic materials are either not durable enough (the case of organic photochromic dyes), or not easily manufactured onto large glass panes (the case of silver halides). The requirements of durability and large area fabrication have hitherto hindered the application of photochromism in smart glazing. Thus, the importance of rare-earth oxyhydrides, which have emerged during the last decade as an inorganic (and hence, in principle, durable) photochromic family of materials that can be prepared onto large area glass panes by magnetron sputtering. In this work, we will discuss in detail the photochromic effect in oxyhydrides, how to prepare and optimize photochromic coatings with excellent switching kinetics, as well as answer other frequently asked questions when it comes to the applications of rare earth oxyhydrides in glazing.

1. Introduction

In 1990 the term *chromogenic* was coined for designating materials that change color in a reversible but persistent manner as a response to an external stimulus [1]. Depending on the nature of the external stimulus e.g., an electrical current, changes in the temperature, the presence of certain gasses or light of certain wavelength, a chromogenic material can be classified within the electrochromic, thermochromic, gasochromic or photochromic category, respectively. The potential that chromogenic materials present as smart adaptative materials for the glazing industry, was identified by C. G. Granqvist [2,3] and C. M. Lampert [4] very early on. Commonly, the term *chromogenics* refers to technologies with applications in dynamic large-area transmittance control, i.e, in smart window glazing [5].

According to a recent report by the International Energy Agency IEA, during operation the existing building stock is responsible of ca. 30% of the global energy consumption and 26% of the global greenhouse gas emissions [6]. In a building, the glazing envelope is typically the Achilles' heel in terms of energy efficiency: windows often leak heat during cold days and admit too much solar energy during hot days, putting unnecessary load on the heating/cooling system [7–10]. Commonly, state-of-the-art windows are static and therefore cannot adapt their optical properties to the weather conditions. This leaves untapped a large energy-savings potential specially in mid-latitudes: static windows can be designed to work efficiently – and they do a very good job – either during summer (solar control windows [11]) or winter (low emittance low-E windows [11]), but not during both seasons [8,10,11]. In colder regions, such as the Nordic countries, current architectural trends favor large-area glazed façades. However, to manage summer conditions effectively, these designs require the use of solar control windows [12]. Typically, this entails the utilization of static glass that transmits as little as ~ 50% of the visible solar radiation [10]. Without the aid of artificial lighting, this results in dim interiors for the majority of the year, especially when solar light is not directly reaching the glazing.

Failing to maximize the use of natural resources, solar light and heat, may impede our progress towards the decarbonization of the building sector [8,9] and hinder the goals set by international treaties such as the Paris Agreement. In this sense, chromogenic materials, are excellent tools for addressing this problem by being the key to dynamic glazing solutions able to regulate on demand the fraction of solar light that passes through the building's glazing envelope and maximize the use of natural resources [8–10,13]. The energy savings provided by chromogenic (electrochromic) glazing are huge and beyond dispute [13–21], potentially reaching up to 170 kWh/(m^2 year) [14].

Among the different chromogenic materials, photochromic materials are arguably the most widely recognized by the public thanks to their signature product: the photochromic ophthalmic lens [10,22]. Following the general definition for chromogenic materials given above,

☆ This paper is affectionately dedicated to Prof. Claes-Göran Granqvist. The contributions by Prof. Granqvist to the field of large-area transmittance control are vast and widely recognized by the research community. We, who know him personally, also know that he is brilliant, witty and, as the poet put it, *a good man in the true sense of the word good*.

E-mail address: jose.montero-amenedo@angstrom.uu.se.

https://doi.org/10.1016/j.solmat.2024.112900
Received 29 December 2023; Received in revised form 23 April 2024; Accepted 27 April 2024
Available online 9 May 2024

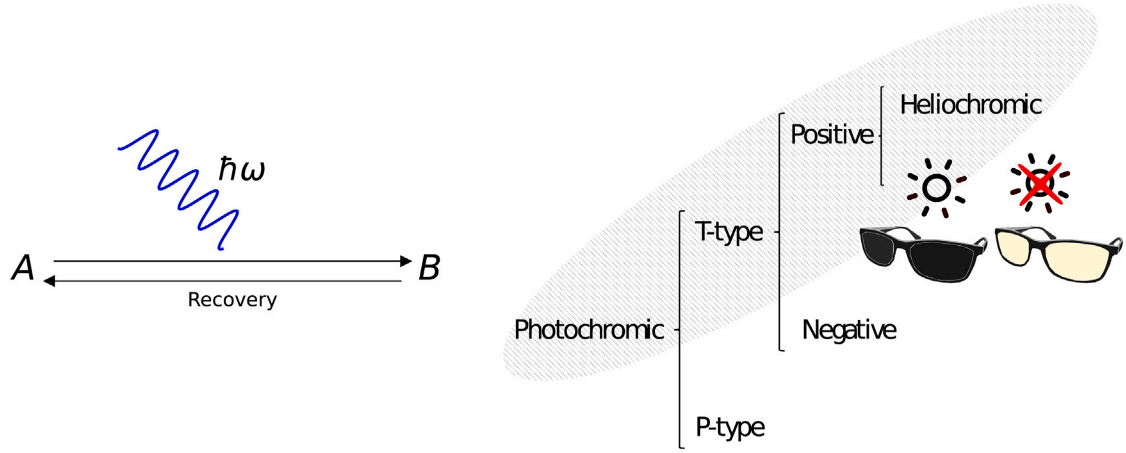

Fig. 1. Left: a photochromic material switches reversibly from a state A to a state B with different optical properties by the action of electromagnetic radiation ($\hbar\omega$). Right: taxonomy of photochromic materials according to A. D. Towns [23]. Most photochromic materials with industrial applications lie within the T-type, positive and heliochromic category, being photochromic eyeglasses (schematically represented in the inset) a notable example of their successful application.

a material is said to be photochromic if it can switch from a state A to and state B – where A and B exhibit different optical properties – by the action of light of adequate energy ($\hbar\omega$) and intensity, see Fig. 1 (left).

For a material to be considered photochromic the change from A to B must be reversible, that is, the material has to be able to return to A from B either by illumination with light of different wavelength (*P-type* photochromism) or simply by thermal relaxation once the illumination has stopped (*T-type* photochromism) [23,24]. A T-type photochromic material is said to exhibit *positive* photochromism if state A exhibit higher transparency than state B, i.e., a positive photochromic material darkens as a response to illumination [23,24]. A negative photochromic material, on the other hand, bleaches under illumination. A. D. Towns [23,24] introduced yet another dimension in this classification: a T-type positive photochromic material is said to be *heliochromic* if it darkens by the effect of solar light. Following these definitions, the taxonomy of photochromic materials is summarized in Fig. 1. Only a subgroup of photochromic materials, those heliochromic, are potentially of interest for large area transmittance control in façade glazing.

The first photochromic product commercially available was based on heliochromic silver-halide silicate glass [25]. Developed in the early 60's at Corning Glass Works, Inc. by W. Armistead and Stookey [22,25], photochromic silver-halide silicate glass was found to be very adequate for the ophthalmic industry. The application was simple but brilliant: prescription glasses that turn into sunglasses under strong illumination (e.g. outdoors in a sunny day) and that return to their original transparent state once the level of illumination decreases (e.g. indoors), see an schematic representation in Fig. 1 (inset). The same idea could be, in principle, applied for regulating the transmittance of the glazing in the façade of a building. At this point the first setback arises: the manufacturing of photochromic silver halide-based glass cannot be seamlessly integrated into the float-glass production process, which is typical for large-area glass panel fabrication [26,27]. Meanwhile, the ophthalmic industry transitioned from silver halides into inorganic photochromic dyes, easier to implement in organic lenses enabling a lighter and less brittle final product [28,29]. Unfortunately, these organic dyes are not suitable either for applications in buildings due to their limited durability, specially under UV irradiation [23]. Indeed, architectural glazing is expected to have a lifespan of at least 30 years, far longer than the lifespan of organic photochromic dyes [23,24]. Other inorganic compounds, e.g. those based on transition metal oxides such as WO_3, often lack of adequate switching speed and contrast [10,30].

While there are various requirements that a photochromic material has to fulfill in order to be suitable for the fabrication of smart glazing, e.g. switching under visible light (not only UV), resilience to high temperature, bleaching even at low ambient temperature, darkening even at high ambient temperature, etc., the possibility of large area fabrication and adequate durability are still the principal challenges that hitherto have hindered the realization of photochromic façade glazing. With photochromism out of the picture, the field of large-area transmittance control is currently dominated by electrochromic devices [31,32]. Still, a hypothetical photochromic glazing would present certain advantages when compared to electrochromic glazing, being its simplicity and hence a reduced fabrication cost the most notable one: whereas a photochromic device requires a single coating to function (the photochromic material itself), a standard electrochromic device requires at least 5 layers (2 transparent electrodes, one ion storage film, an electrolyte and the electrochromic material) plus a control unit and a source of electricity [9,29,33]. In light of the above, assuming a similar light transmission control, the energy savings provided by a photochromic device would be more cost effective than those provided by an electrochromic device.

What role do rare earth (RE) oxyhydrides play in this context? As it will be discussed in detail, RE oxyhydrides emerged fairly recently [34] as a new group of materials exhibiting a dramatic photochromic response (T-type positive heliochromic) combined with high transparency in the clear state. Due to their inorganic nature, RE oxyhydrides are expected to exhibit a certain degree of stability. Moreover, RE oxyhydrides can be deposited at industrial scale by sputtering [35,36], following the usual protocols for the coating of large-area glass surfaces [37]. Thus, for transmittance control in facade glazing applications, RE oxyhydrides have the possibility to become a game-changing technology.

The first reference to photochromic RE oxyhydrides corresponds to yttrium oxyhydride YH_xO_y, hereinafter referred for simplicity as YHO (same notation will be applied to other compounds, e.g., GdHO, NdHO, etc.). Photochromism in YHO thin films was discovered by T. Mongstad et al. [34] when attempting to prepare yttrium hydride films by magnetron sputtering in an argon and hydrogen plasma. A visual inspection of the films, once removed from the deposition chamber, revealed that they looked nothing like YH_2. While, as we will see, YH_2 (or more precisely the dihydride β-YH_2 phase) has a metallic character and hence it is essentially opaque [38], the obtained samples were completely transparent, exhibiting a relatively wide band gap (2.6 eV) [34] of energy between metallic YH_2 and the larger band gap observed in Y_2O_3 (5.6 eV) [39]. In addition, the composition of the samples indicated a large content of oxygen as well as remarkable photochromic properties, see Fig. 2 upper panel. Later this compound was identified as an oxyhydride [40], that is, a mixed-anion compound

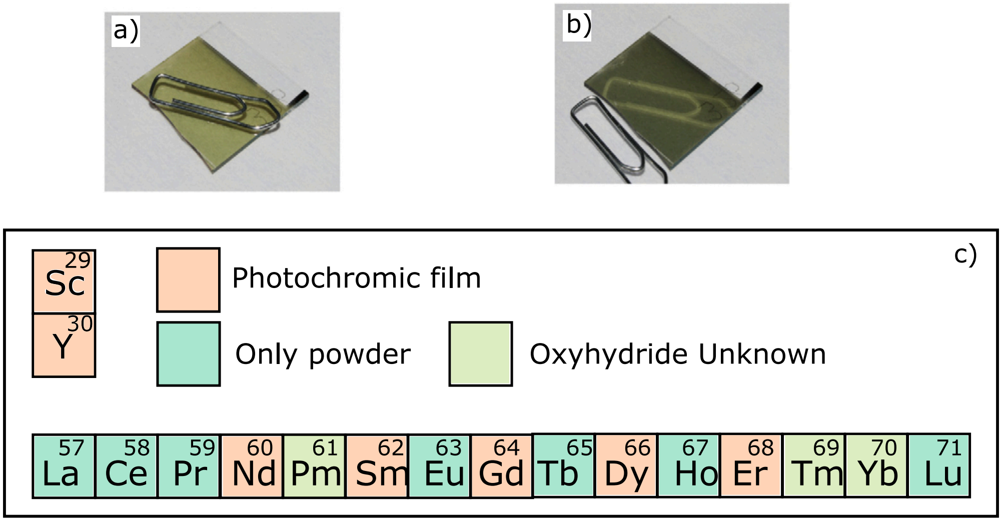

Fig. 2. Top panel: photographs of a 500 nm-thick YHO film from the seminal paper by T. Mongstad et al. [34]. The film before illumination is shown in panel (a), and after illumination in panel (b). The paper clip was used as mask during illumination to highlight the optical switching. Reproduced from Ref. [34] with permission from Elsevier. Panel (c) shows rare earth elements classified in three categories: *(i)* those from which photochromic oxyhydride films have been obtained, *(ii)* bulk oxyhydrides of unknown photochromic properties and *(iii)* rare earth elements from which an oxyhydride phase has not been reported.
Source: Adapted from D. Chaykina et al. [42] (CC-BY).

in which oxide and hydride anions coexist in a single phase [41]. Follow up works resulted in the discovery other photochromic RE oxyhydrides, where RE = Sc, Nd, Sm, Gd, Er and Dy [35,42–44]. Bulk powder oxyhydrides have been reported also for La, Ce, Pr, Tb, Ho, Er and Lu [45–50] (Fig. 2 lower panel), although their photochromic properties are unknown [42].

The present work is organized as follows: in Section 2 we will describe in detail the fabrication process of photochromic REHOs, while in Section 3 we will study some fundamental aspects of the photochromic and related issues such as transparency in the clear state, photochromic contrast, bleaching kinetics as well their dependence on deposition conditions and on the choice of the particular cation (Y, Sc, Nd, Sm, Gd, Er and Dy). Note that some REHOs such as YHO have been much more studied than others (e.g. SmHO, ErHO) and hence, in this work, some aspects are discussed using YHO (and/or sometimes GdHO) as reference, assuming that the physico-chemical properties of lanthanide-based compounds are very similar to those compounds formed by Y or Gd [35,38,42].

2. Synthesis

RE dihydrides REH_2 (β-phase) constitute the scaffold on which the oxyhydride phase can be built. For this reason, before getting into a detailed explanation of the synthesis process, it is convenient to get acquainted with the phase diagram of the RE–H system (Fig. 3) [38]. We would rely on this knowledge for some discussions later on. As mentioned before, photochromism has been reported in REHO thin films being RE = Y, Sc, Nd, Sm, Gd, Dy, Er. Starting from a metallic phase (α-phase), these elements form a face-centered cubic *fcc* fluorite-type dihydride phase (β-phase) that coexist with the α-phase until a stoichiometry REH_δ with $\delta \sim 2$ is achieved [38]. Further hydrogenation leads to the formation of an hexagonal trihydride phase (γ-phase), except in the case of Nd where the trihydride also exhibits a cubic fluorite structure [38]. Regarding the electrical properties, both β-phase and the α-phase present metallic-like properties, whereas the γ-phase behaves as a wide band gap semiconductor [38]. Hexagonal trihydrides subjected to pressures above several gigapascals can switch to a high-pressure *fcc* phase, usually considered not stable at ambient pressure [51,52].

Based on the standard Gibbs free energy of formation, Y, Sc, Nd, Sm, Gd, Dy dihydrides are some of the most stable transition metal hydrides [38]. Among them, YH_2 stands out, being able to retain hydrogen even at relatively high temperatures [53]. Thus, not surprisingly, the first photochromic REHO reported was YHO [34]. Interestingly, before the discovery of photochromism in oxyhydrides, A. Ohmura et al. [52] reported photochromic properties in γ-YH_3 (kept at room temperature and at hydrogen pressures of several GPa) based on the metal-to-insulator transition that takes place from the $\beta-$ to the $\gamma-$phase.

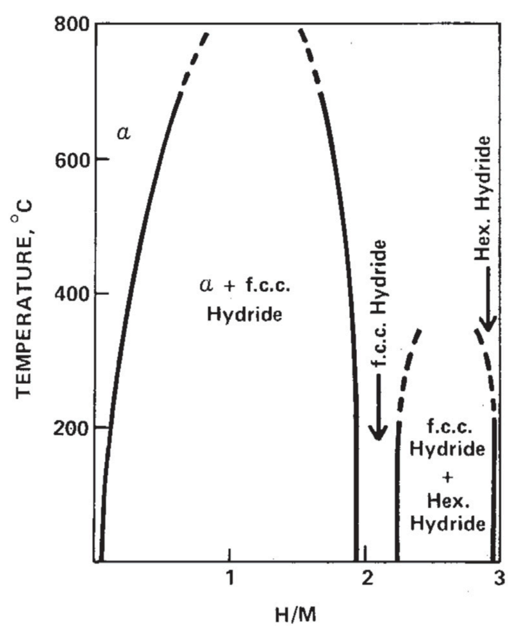

Fig. 3. Phase diagram of the RE/H system.
Source: Reprinted from Ref. [38] with permission from Elsevier.

Achieving REH_3 typically require injection of hydrogen into rare earth metals subjected high pressure [38,52,55] and hence, to our knowledge, REH_3 films cannot be achieved by sputtering [55]. Thus, the synthesis by sputtering of REHO oxyhydrides begins with the deposition of REH_2 precursor films, which can be achieved in an argon

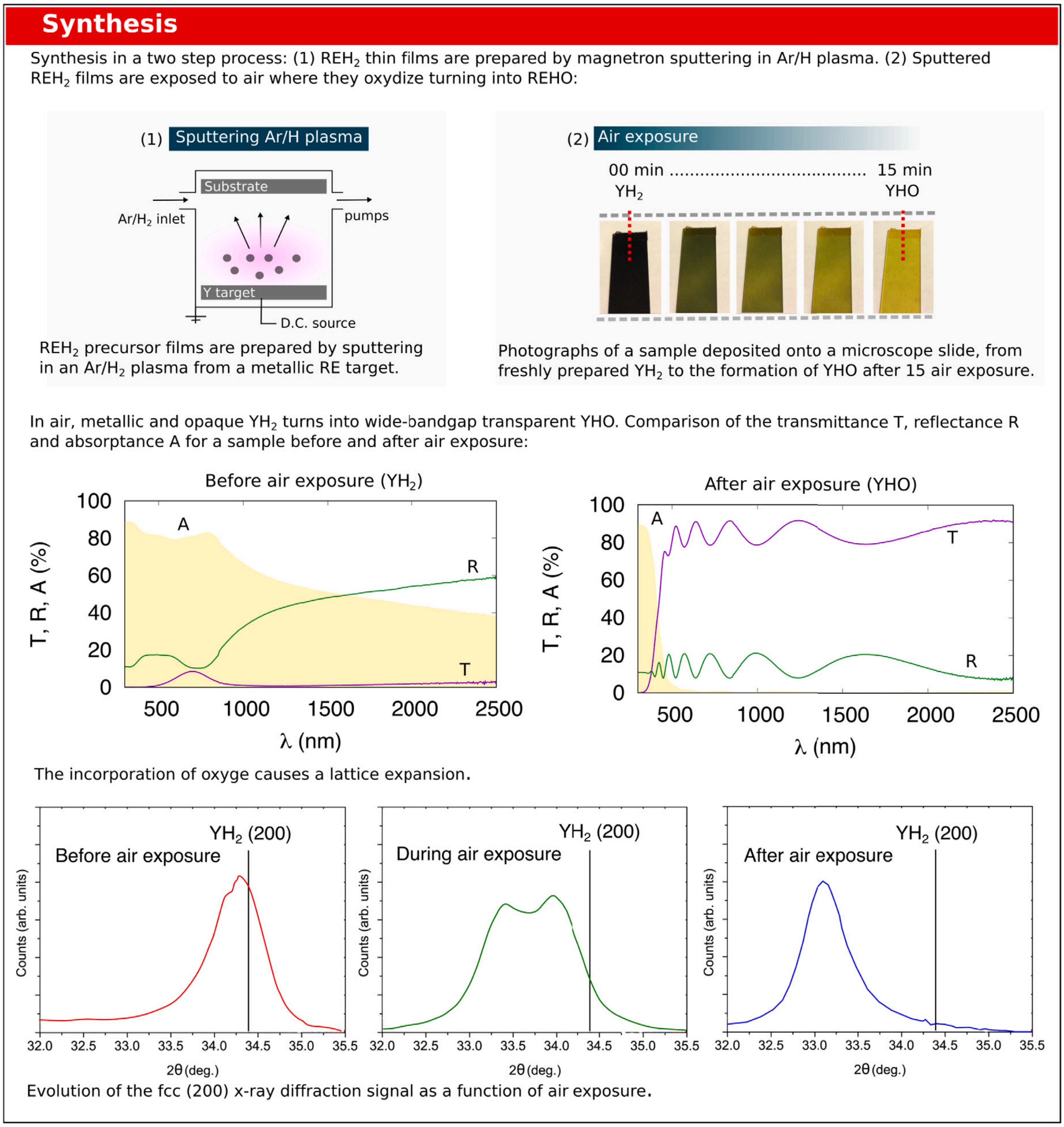

Fig. 4. The synthesis process consist typically in two steps,: deposition of REH_2 precursors by sputtering followed by their air exposure for oxygen incorporation (top). The incorporation of oxygen leads to the band gap opening (middle) and lattice expansion (bottom). Middle panel from E. M. Baba et al. [54] (CC-BY), bottom panel adapted from J. Montero et al. [36] with permission from Elsevier.

and hydrogen plasma without intentional substrate heating [36]. This route was the approach taken by T. Mongstad et al. [34] in their first report of a photochromic oxyhydride. However, the specific details (determination of the precursor phase and phase transformation) were described later by J. Montero et al. [36] and F. Nafezarefi et al. [35]. Given the electrical conductivity of REH_2, the process can be carried out by DC or pulsed-DC sputtering using a metallic RE target, achieving relatively high deposition rates, Fig. 4 top panel (left). In the literature, the deposition of the REH_2 precursor is achieved in a wide range of Ar/H_2 flow ratios, e.g. 10:1 [36], 7:1 [42], 2:1 or 1:1 [56]. As we shall see, although for a given set of deposition conditions there is probably an optimum Ar/H_2 flow ratio [56], the parameter that most significantly influences the final properties of the photochromic samples is the sputtering pressure.

For the formation of photochromic REHO, the REH_2 precursor films are exposed to air, where opaque metallic-like REH_2 transform into electrically highly-resistive [57,58] transparent photochromic REHO [36]. Simplifying, for an stoichiometry REH_xO_y where $x = 1$ and $y = 1$, the reaction can be written as follows [44] :

$$REH_2 + \frac{1}{2}O_2 \rightarrow REHO + H\uparrow . \quad (1)$$

In agreement with Eq. (1), ion beam analysis revealed that oxygen and hydrogen content are inversely correlated in photochromic YHO films [59,60]. Note that Eq. (1) is a simplified version of a more complex process described in Ref. [44]. Also, depending on the final stoichiometry of the oxyhydride, the release of hydrogen in Eq. (1) may not be necessary, thanks to the multi-valence of Y [54]. A sequence of photographs capturing the transformation of REH_2 into REHO, being RE = Y is shown in Fig. 4 top panel (right). The photographs shown in Fig. 4 were taken in a time interval of 15 min, however, as we

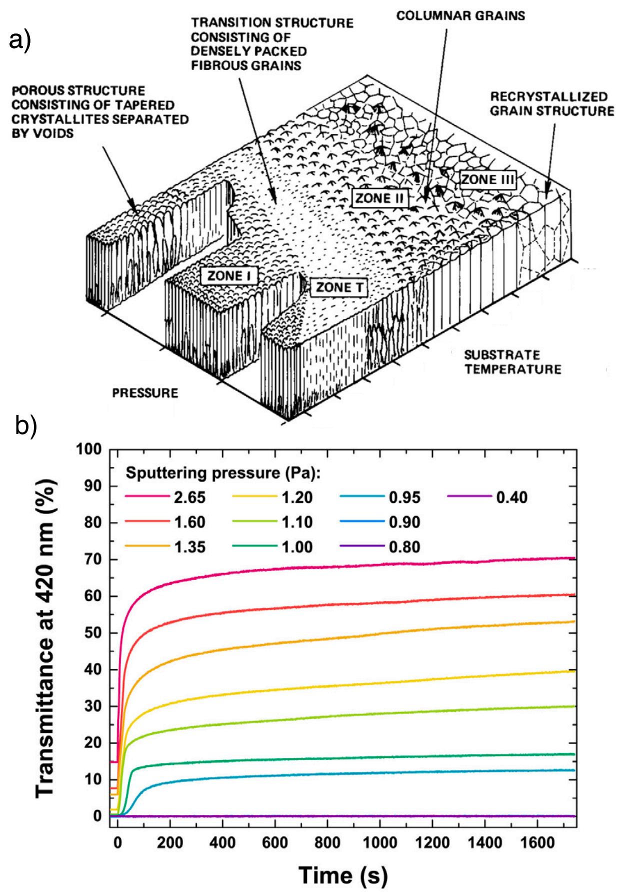

Fig. 5. Panel (a): Thornton diagram of sputtering zones, reproduced from Ref. [62] with permission from AIP. Panel (b): evolution of the transmittance at a wavelength of 420 nm as the precursor films, deposited at different pressures, are exposed to oxygen. Panel (b) reproduced from M. Zubkins et al. [56] with permission from Elsevier.

will see, the time frame of the reaction described by Eq. (1) can vary largely depending on the deposition conditions. Usually photochromic REHO films reported in the literature have thicknesses ranging from hundredths of nanometers to several micrometers [61].

The optical transmittance T(λ), reflectance R(λ) and absorptance A(λ) as a function of wavelength λ corresponding to a unreacted (left) and reacted (right) precursor film (RE = Y) of thickness ~ 1.4 μm is depicted in Fig. 4, middle panel. In the unreacted film, the optical properties correspond very well to those expected in YH_2, namely high R(λ) in the near infrared region (signature of the presence of free conducting electrons) and T(λ) = 0 (except for a small bump at 500 < λ < 1000 nm commonly observed in the transmittance trace of rare earth hydride thin films approaching the stoichiometry REH_2 where RE = Y, Gd, Dy, Er [35] as well as in La-Y dihydrides [63]).

After air exposure, the incorporation of oxygen causes the dramatic increase of T(λ) in detriment of A(λ) and R(λ). Interference maxima and minima, signature of a transparent thin film, appear in T(λ) and R(λ), whereas A(λ) is restricted to the fundamental interband transition region (~ 3.3 or 2.6 eV considering a direct or indirect allowed transition for YHO [64]). From a structural point of view, as the REH_2 film turns into REHO, the lattice expands significantly by the incorporation of oxygen. Fig. 4 bottom panel shows the evolution of the X-ray diffraction peak corresponding to the [200] direction of the *fcc* crystalline structure in YH_2 during air exposure [36]. For comparison, the vertical line in the graphs represent the position of the (200) diffraction line according to the ICDD card num. 04-002-6938 corresponding to YH_2. The diffraction peak displaces noticeably towards smaller angles, pointing to a substantial increase of the interplanar distance as YH_2 turns into YHO. This corresponds to an increase of the lattice constant *a* from ~ 5.2 to 5.4 Å as YH_2 turns into YHO [36]. Contrary to some observations in the literature [65], the REHO and REH_2 phases can be clearly differentiated by X-ray diffraction, Fig. 4 bottom panel. In the case of yttrium oxydeuterate the lattice constant, as determined by M. H. Sørby et al. [66] by neutron diffraction, expands from 5.19 Å to 5.32 Å as YD_2 turns into YDO. Theoretical studies suggest that, in the REHO structure, O^{2-} occupies tetrahedral positions while H^+ can occupy both tetrahedral and octahedral positions [67].

The kinetics of the process described in Eq. (1) is greatly determined by the chamber pressure during the sputtering deposition of the precursor REH_2. Taking as a reference the classic diagram of sputtering deposition regions by Thornton [62], Fig. 5(a), at low deposition temperatures there is a given critical pressure P_c above which the deposition regime switches from Zone T (densely packed grains) to Zone 1 (porous structure). Porosity is a crucial parameter and thus precursors must be deposited above P_c to ensure the correct incorporation of oxygen [35]. F. Nafezarefi et al. [35] determined P_c to be 0.4 Pa for the deposition of YHO, and slightly larger (P_c= 0.6 Pa) for GdHO, DyHO and ErHO oxyhydrides. G. Colombi et al. [44] determined P_c = 0.3 Pa for ScHO while D. Chaykina determined P_c ~ 0.6 Pa for SmHO. Note that these values may depend on the particularities of each coater (geometry, distance target-substrate, etc.) as well as other parameters such sputtering power density.

Fig. 5(b) shows the evolution of the transmittance at a wavelength of 420 nm of different REH_2 precursor films (RE = Y) as a function of time exposure to pure oxygen (5 N), from M. Zubkins et al. [56]. The transmittance at such wavelength is a good indicator of the opening of the band gap and hence of the incorporation of oxygen in the lattice of the precursor film. In this sense, it can be observed that the rate at which oxygen is incorporated increases with the sputtering pressure. While samples deposited at high pressures (e.g., 2.65 Pa) react in few seconds, films prepared at low pressures take longer time, or not react at all (e.g., the films deposited at 0.40 Pa) [56]. Controlled exposure to pure oxygen shows that porous films [68] require lower oxygen dosages to achieve photochromic properties than more compact films [56]. As we will see next, the oxidation process continues when the films are exposed to air, being the most porous films more susceptible to degradation. One of the differences between films exposed to air when compared to films only exposed to pure oxygen is the emergence of O–H bonds after air exposure, as observed by Fourier-transform infrared spectroscopy [56]. The implications of the O–H bonds in the photochromic properties have not been investigated yet.

D. Moldarev et al. [69] determined the atomic ratios of O/H and O/Y in two YHO films on which the hydride precursors were prepared by magnetron sputtering at 1.0 and 6.0 Pa, maintaining the Ar and H_2 ratio constant (40 and 160 sccm for H_2 and Ar, respectively). The obtained results, presented in Table 1, confirmed that high deposition pressures result in porous films with higher oxygen content. Besides, as described by Eq. (1), as oxygen atoms are incorporated in the material, the content of hydrogen decreases. Moreover, Table 1 shows that the films keep oxidizing and loosing hydrogen even 7 months after air exposure being this change more dramatic in films deposited at high pressures. Additional studies by G. Colombi et al. [44] in REHO (RE = Sc, Y and Gd), confirmed that the deposition pressure during the fabrication of the REH_2 precursors determines the final oxygen content in the oxyhydride, even in a pressure range closer to P_c. How all these parameters affect the final transparency and photochromic properties of REHOs will be discussed in next sections.

In addition to deposition pressure, the geometry, target size, and other characteristics of each sputtering coater will determine the optimal set of deposition conditions, including applied power to the target. Static deposition of RE_2 precursor films in large area coaters may result in precursor films exhibiting a *deposition zone gradient* which can lead to an uneven incorporation of oxygen, see C. C. You et al. [60,70].

Table 1
O/H and H/Y atomic ratios corresponding to two different REHO samples (where RE = Y) as a function of time exposure to air. The sample precursors were prepared by sputtering at 1.0 and 6.0 Pa, respectively.
Source: Reprinted from D. Moldarev et al. [69] with permission from Elsevier.

Deposition pressure	1.0 Pa			6.0 Pa		
Time exposed to air	1 week	2 months	7 months	1 week	2 months	7 months
O/H	1.0	1.1	1.3	1.7	2.0	2.1
H/Y	2.2	1.7	1.4	0.6	0.7	0.8

It is important to highlight that the low-temperature deposition process followed for the fabrication of photochromic REHOs (the substrate is not intentionally heated and the deposition power density applied to the RE target can be kept as low as 1.33 W/cm^2 [36]), allows the synthesis onto webs, enabling roll-to-roll deposition and the fabrication of photochromic membranes which can be used as standalone devices or for glass lamination. This provides easy ways of transportation (plastic is much lighter and less brittle than glass, implying less CO_2 emissions and lower costs), resulting in a positive impact on the life-cycle analysis of the final photochromic product [9].

The lattice expansion, caused by the incorporation of oxygen, observed in Fig. 4 bottom panel can often lead to flaking and delamination of the film. For this reason, a proper cleaning and/or conditioning of the substrate is very important. For the deposition onto glass substrates, it is advisable to start by washing the substrates with a mild soap solution and removing any visible contamination with a sponge. Then, rinse the substrates with deionized water removing any soap residue and subsequently blow them dry. Follow by soaking the substrates during few minutes in acetone to remove any remaining organic residues and rinse them again with deionized water. Next, wipe them with a lint-free cloth soaked in isopropyl alcohol, rinse with deionized water and blow dry. For particularly dirty substrates, use ultrasonic agitation (sonication) in a bath of isopropyl alcohol or deionized water to dislodge any remaining particles or contaminants from the substrate surface. Achieving good adherence onto some substrates, such as Sn:In_2O_3 ITO coated glass is, in our experience, particularly challenging. This may be caused by the larger surface roughness of ITO, which prevents an intimate contact with the precursor hydride, leading to delamination when the lattice expands as the oxyhydride is formed.

3. Photochromic effect

Next, we will discuss the effect of the deposition pressure and film thickness on the transparency and photochromic contrast of REHOs (Section 3.2). Also, we will describe how the election of the cation (Y, Gd, Dy, etc.) could ultimately influence the functional properties of the REHO films, Section 3.3. In Section 3.4, we will investigate which wavelengths are able to trigger the photochromic effect, while in Section 3.5 we will discuss about haze and color perception, which are essential features in glazing applications. Durability, delamination and capping will be addressed in Section 3.6.

However, before scrutinizing in detail these specific aspects, and in order to get acquaintance with the photochromic effect in REHOs, we will first introduce in Section 3.1 some of its basic features. These, as summarized in Fig. 6, are: solar and visible light modulation, optical band gap and transparency, a brief discussion of a model for explaining the observed light-induced darkening, as well as some words on the reversibility of the photochromic effect.

3.1. Basics

Solar and visible light modulation

The transmittance trace T(λ) of a typical photochromic REHO, before and after illumination, is shown in Fig. 6 left column top panel. In this particular case, the data shown corresponds to total transmittance (includes direct, but also possible scattered light, measured in a Perkin-Elmer Lambda 900 spectrophotometer equipped with an integrating sphere) of a 1.5 μm-thick GdHO film deposited onto glass. The transmittance in the dark state was measured after illumination with a LED source during 15 h (λ = 365 nm, power 27 mW/cm^2). Since, as we will discuss later on, light scattering is negligible in these films, the use of an integrating sphere is facultative. By comparing this transmittance data with both the spectral distribution of the solar irradiance at the earth surface φ_{sol} [71] and the relative efficiency of the human eye φ_{lum} [72] (Fig. 6, left column middle and bottom, respectively), we can draw the following conclusions: *(i)* REHO coatings block, both in the clear and photodarkened state, the solar UV radiation (λ < 300 nm), which is harmful for our eyes and skin, but also for the objects that are usually kept indoors, e.g., furniture, fabrics, paintings, etc. Note that ordinary window glass alone transmits some UVA radiation [73]. *(ii)* The photochromic optical modulation in REHOs occurs not only in the visible part of the solar spectrum (400 nm < λ < 700 nm), but also in the infrared (700 nm < λ < 2500 nm). *(iii)* The decrease in transmittance is quite homogeneous in the visible range, so REHOs keep color neutrality when photodarkened. Points *(ii)* and *(iii)* must not be taken for granted, e.g. silver halide glasses, as well as many organic dyes, switch mostly in the visible region, but not so much in the NIR [10,23,74]. On the other hand, photochromic tungsten oxide switches in the long-wavelength range of the visible spectrum (red), resulting in deep-blue colored photodarkened films [10,30].

Transparency and modulation of the visible and solar radiation are fundamental characteristics of smart window glazing. Those can be summarized in two parameters: the solar transmittance T_{sol}, and the luminous transmittance T_{lum} which are often used by the industry for the characterization of architectural glass [75]. T_{sol} and its photochromic modulation ΔT_{sol} can be defined as follows:

$$T_{sol} = \frac{\int d\lambda\ T(\lambda)\ \varphi_{sol}(\lambda)}{\int d\lambda\ \varphi_{sol}(\lambda)}, \tag{2}$$

and

$$\Delta T_{sol} = T_{sol}\ (\text{clear}) - T_{sol}\ (\text{dark}), \tag{3}$$

where T_{sol} (clear) and T_{sol} (dark) refer to T_{sol} calculated in the clear (before illumination) and dark (after illumination) state. Analogously, we can obtain T_{lum} and its photochromic modulation ΔT_{lum} simply by substituting φ_{sol} by φ_{lum} in Eqs. (2) and (3).

According to these definitions, for the aforementioned GdHO coating, the obtained T_{sol} is 65% and 15% in the clear and photodarkened state, respectively, i.e., $\Delta T_{sol} \sim$ 50%. Regarding the visible part of the spectrum, the coating also provides large modulation, being $\Delta T_{lum} \sim$ 52%, combined with relatively large transmittance in the visible region in the clear state ($T_{lum} \sim$ 66%).

Without focusing on these exact values of ΔT_{sol} and ΔT_{lum}, which depend on many factors (sample composition, temperature, illumination source, illumination time, etc.), we can conclude that the photochromic switching in REHOs has the adequate spectral distribution to provide dynamic control of both T_{sol} and T_{lum}. Considering the optical switching properties as seen in Fig. 6 (left column), when implemented in architectural glass, REHOs can potentially provide thermal comfort, decrease the cooling demand during sunny days, as well as prevent glare. On the other hand, during dark cloudy days, the REHO coating can remain in the clear state, admitting as much natural light and solar radiation as available, decreasing the heating demand and the need for artificial lighting.

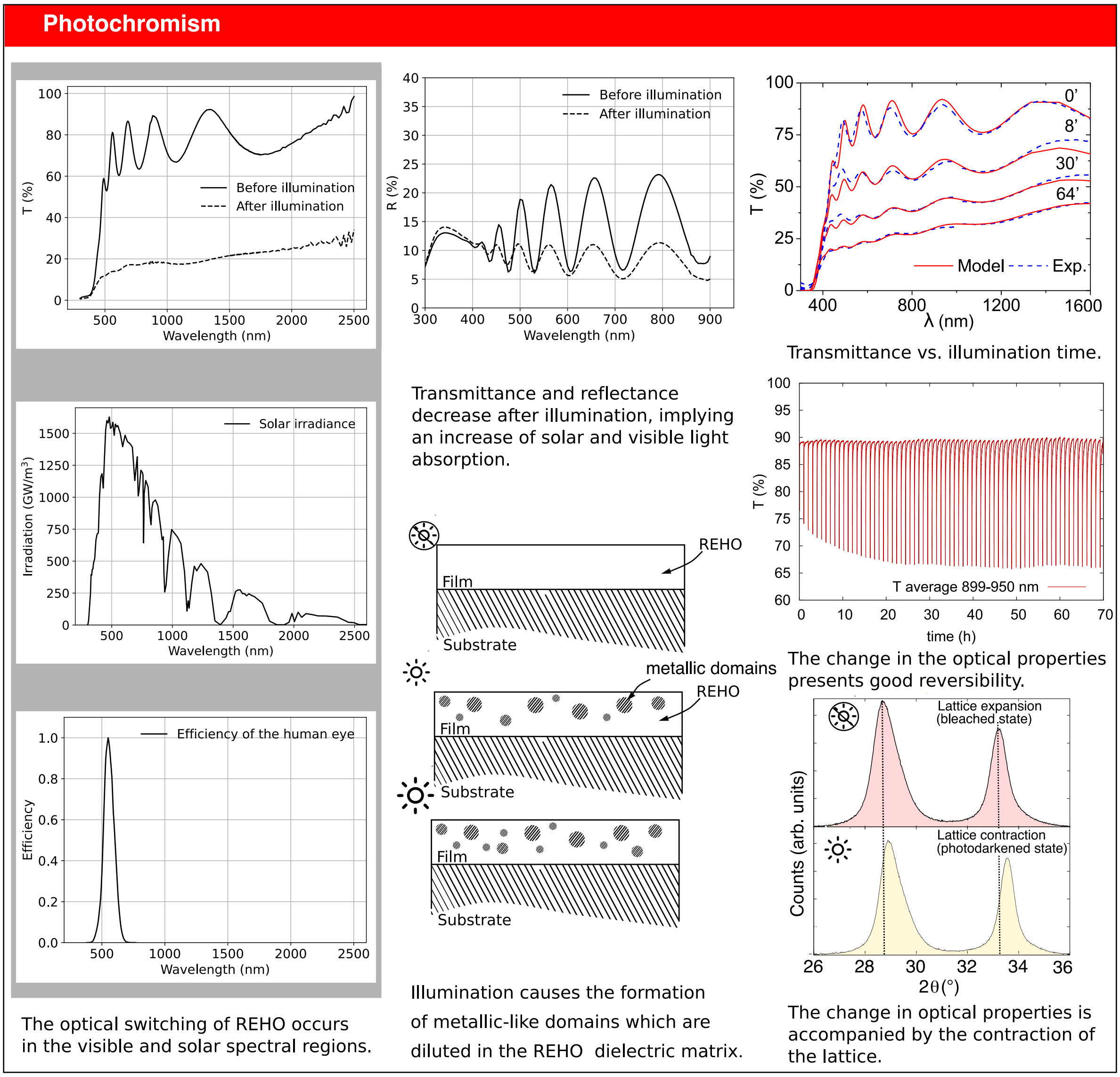

Fig. 6. The column on the left shows the optical transmittance T(λ) corresponding to a GdHO sample before and after illumination (top), the solar irradiance at the Earth's surface (middle) and the relative efficiency of the human eye (bottom), all as a function of wavelength. Middle column shows the reflectance R(λ) of a YHO film before/after illumination (top) and a schematic representation of the diluted metallic-domain DMD model (bottom). The DMD model works very well in predicting the changes in T(λ) vs. illumination time in YHO (right column, top). T(λ) averaged between 899 and 950 nm under light/darkness cycles for a YHO film is shown in the column on the right (middle). XRD patterns corresponding to clear/dark states in YHO are shown the column on the right (bottom). Right column top reproduced from J. Montero et al. with permission from Wiley. Right column middle and bottom reproduced from J. Montero et al. [61] with permission from AIP Publishing and E. Baba et al. [54] (CC-BY).

In terms of energy efficiency the parameters T_{sol} and ΔT_{sol} can give a good estimate of the energy performance of REHO coatings. Alternatively to T_{lum} and T_{sol}, in the literature we often find T(λ) and its photochromic change ΔT(λ) averaged in different regions such as in the visible or near infrared spectral range.

Band gap, transparency and optical absorption

In the visible region (400 < λ < 700 nm equivalent to $1.7\text{eV} < \hbar\omega < 3.0$ eV), far from phonon resonances (typically occurring in the midthermal range [76]) and without free electrons which can cause Drude-like absorption [77], REHOs remain mostly non-absorbing and hence optically transparent in the non-photodarkened state. However, band gap absorption and Urbach tails can penetrate slightly into the visible region at short wavelengths causing some absorption. Fortunately, the band gap transition is most likely indirect, which reduces further the effect of this optical absorption in the visible region [78]. In the literature we can find the following optical band gap values (indirect allowed unless stated otherwise): 2.5–2.6 eV and 3.0–3.3 (direct allowed) for YHO [64], 2.8 to 3.7 for YHO (direct allowed) [79], 2.0 to 2.2 eV for NdHO [43], 2.0 to 2.2 eV for SmHO [42], 2.2 to 2.5 eV for ScHO, YHO and GdHO [40], 2.2 for DyHO and 2.04 for ErHO [35]. These values ensure a high T_{lum} in the clear state in most cases.

On the other hand, REHOs become optically absorbing in the photodarkened state. Fig. 6, middle column top panel, shows the reflectance $R(\lambda)$ for a YHO film before and after illumination. Same as before, it is also total reflectance measured using an integrating sphere in a Perkin-Elmer Lambda 900 spectrophotometer. Illumination in REHOs causes the decrease of T(λ), but also of R(λ). Since energy conservation dictates:

$$T(\lambda) + R(\lambda) + A(\lambda) = 1, \tag{4}$$

thus, the photochromic modulation occurs at the expenses of an increased optical absorbance A(λ). This has several implications: *(i)* under strong solar light, REHOs will become absorbing, largely increasing their temperature. *(ii)* As it will be discussed later on in detail, this temperature raise will have an impact on the photochromic kinetics and contrast of the film. *(iii)* When applied onto glazing, the use of tempered glass, for a larger resistance to thermal stress, may be recommended, as it is usual in electrochromic glazing [80] which also become absorbing in the dark state. *(iv)* Although T_{sol} may be largely reduced, the total solar heat gain coefficient (understood as the fraction of solar radiation admitted through the coating, either directly transmitted or absorbed and re-radiated indoors [81]) may not decrease as much as expected. In order to overcome this problem, in glazing applications REHOs need to be implemented in combination with Low-E coatings such as transparent conductors or very thin silver coatings [76,77,82].

The dilute metallic-domain DMD model

The first model for explaining the photodarkening in REHOs was the dilute metallic-domain DMD model [36,61]. The DMD model assumes that, during illumination, metallic domains grow embedded in the REHO transparent film. Rather than forming a continuous layer, these domains occupy a volume fraction or filling factor f, being f in the dilute limit ($f \ll 1$). Therefore, the optical properties of the resulting composite may be modeled using the Maxwell–Garnett effective medium approximation [83,84]. On this basis, starting from $f = 0$ in the transparent state (no metallic phase present in the film), f grows gradually under illumination, causing the increase of $A(\lambda)$ [36,61]. This model is schematically presented in Fig. 6 middle column, bottom. It is important to underscore that the formation of a continuous metallic layer would result in increase $R(\lambda)$ rather than an increase of $A(\lambda)$, specially for λ in the infrared (below the plasma frequency, which depends on the number of conducting electrons per volume) [11,77]. This suggests that the photochromic effect is inherent to the whole volume of the film, rather than being limited to the film's surface [61]. However, when photochromic contrast is tested in relatively thick films by using monochromatic light of short wavelengths, a *skin effect* can be observed [85,86] inherent to the penetration depth of the incident beam. For example, in a typical YHO film (thickness ~ 1 μm) the usual extinction coefficient[1] $\alpha(\lambda)$ at $\lambda = 400$ nm is ~ 32685 cm^{-1}. According to Beer–Lambert's Law, 300 nm deep into the sample the intensity of the incident beam drops by a factor $1/e$, i.e., by 37%. The penetration depth can be even smaller if the incidence of the light beam is not normal to the surface of the film.

Back to the DMD model, according to the Maxwell–Garnett approximation, the dielectric function ε of the REHO film at any photodarkening state depends on three factors: the dielectric function of the matrix ε_m in which the metallic domains are embedded (that is, the dielectric function of the film in the clear state), the dielectric function of the metallic domains ε_p and f. Both ε_m and ε_p can be determined experimentally by variable angle ellipsometry: ε_m in a REHO film before illumination, and ε_p by assuming it to be similar to the dielectric function of a non-reacted metallic film deposited at $P < P_c$ [36,61]. This leaves f as the only parameter susceptible of changing under illumination. For our previous work [36], we tested the dielectric function corresponding to an oxygen- and hydrogen-deficient YHO and to the dihydride YH_2 phase, both of metallic character, as possible candidates for ε_p. We achieved a superior fit with the former, while the results obtained for the dihydride YH_2 phase were not published.

The DMD model has been proven to work very well for reproducing $T(\lambda)$ at different photodarkening stages assuming metallic domains of spherical shape in YHO samples deposited at pressures far from P_c. For example, Fig. 6 right column (top) shows the experimental evolution of $T(\lambda)$ as a function of illumination time (0, 8, 30 and 64 min of illumination with a broadband light source EQ-99XFC LDLS) of a film prepared at 1.0 Pa [36]. According to the DMD model, these photodarkening levels can be explained by the increase of f vs illumination time from $f = 0.00$ (0 min.) to 0.02 (8 min.), 0.04 (30 min) and finally to 0.06 after illumination during 64 min [36].

The formation of metallic domains as proposed by the DMD model, is commonly accepted and proven experimentally by several authors [87–90]. The DMD model is also compatible with the persistent photoconductivity observed in REHOs after illumination [34,70,86,91], and with the emergence of Ruderman–Kittel–Kasuya–Yosida RKKY magnetic interactions in GdHO films after illumination [58]. The strong, repeatable photoresponse in the electrical resistivity observed in REHOs opens up new application opportunities beyond smart glazing, including the development of light sensors and other optoelectronic devices [88].

Why these metallic domains are formed by the effect of illumination – or in other words, what are the factors behind the photochromic effect in REHOs – is not completely understood and, although some theories can be found in the literature [54,92], their discussion lies outside the scope of the present work.

Reversibility and memory effect

This brief introduction to the photochromic effect in REHOs would be incomplete without commenting on its reversibility. To reiterate, for a material to be considered photochromic, the optical change has to be reversible. On this basis, Fig. 6 right column middle panel shows $T(\lambda)$ averaged in the interval $899 < \lambda < 950$ for a YHO film subjected to cyclic illumination (the sample was subjected to 1 min illumination with a $\lambda = 405$ nm laser, followed by 59 min of darkness. This cycle was repeated 70 times), as presented by J. Montero and S. Zh. Karazhanov [61]. This film exhibits excellent reversibility. Also, a *memory effect* is observed since the optical contrast increases every cycle during the first 30 cycles [61], as confirmed by other authors [55]. It is also worth mentioning that under cyclic illumination, the lattice of the oxyhydride contracts/expands [54,93], as illustrated by the X-ray diffraction patterns presented in Fig. 6 in the right column, bottom panel, see Ref. [54].

3.2. Deposition pressure and thickness

In photochromic REHOs, the deposition pressure P used during the sputtering process has a large influence on the final transparency and photochromic contrast. This is because, as previously discussed, P has a direct impact on the O/RE atomic ratio [44,69,94,95].

Fig. 7(a) shows $T(\lambda)$ averaged in the wavelength range between 500 and 900 nm ($T_{500-900}$), both in the clear and dark state, for YHO films deposited onto glass at different P values. The optical contrast, represented by $\Delta T_{500-900}$ (achieved after 1 h illumination with a solar simulator) is also included. These particular films were prepared at P ranging from 1.2 to 6.0 Pa by C. C. You et al. [79]. The thicknesses d were 1290 nm, 1220 nm, 1300 nm and 870 nm for the films deposited at 1.2, 2.0, 3.0 and 6.0 Pa, respectively. From Fig. 7(a) it is possible to conclude that increasing the deposition pressure causes an increase in the transparency in the clear state but a decrease of the photochromic contrast. Or, in other words, the larger the oxygen content, the more transparent the film but the smaller the optical switching.

Accordingly, a compromise must be achieved: a large enough oxygen content in the film is needed to ensure transparency, while the content of oxygen has to be low enough to ensure photochromic contrast. Importantly, P is the key parameter to regulate the oxygen content. We note that the sample prepared at $P = 1.2$ Pa and $d =$ 1290 nm, is capable of combining a large transparency in the visible region $T_{lum} \sim 83\%$, with a large photochromic contrast $\Delta T_{lum} \sim$ 22% [79].

The thickness d of the films is yet another parameter to consider. J. Montero and S. Zh. Karazhanov [61] studied the impact of d in T_{lum} and ΔT_{lum} (after 1 h illumination with a solar simulator) achieved by YHO films prepared at $P = 1.0$ Pa, Fig. 7(b). Additionally to experimental data, Fig. 7(b) also shows predictions of T_{lum} and ΔT_{lum} according to the

[1] Calculated for the total transmittance and reflectance of the YHO film shown in Section 3.5.

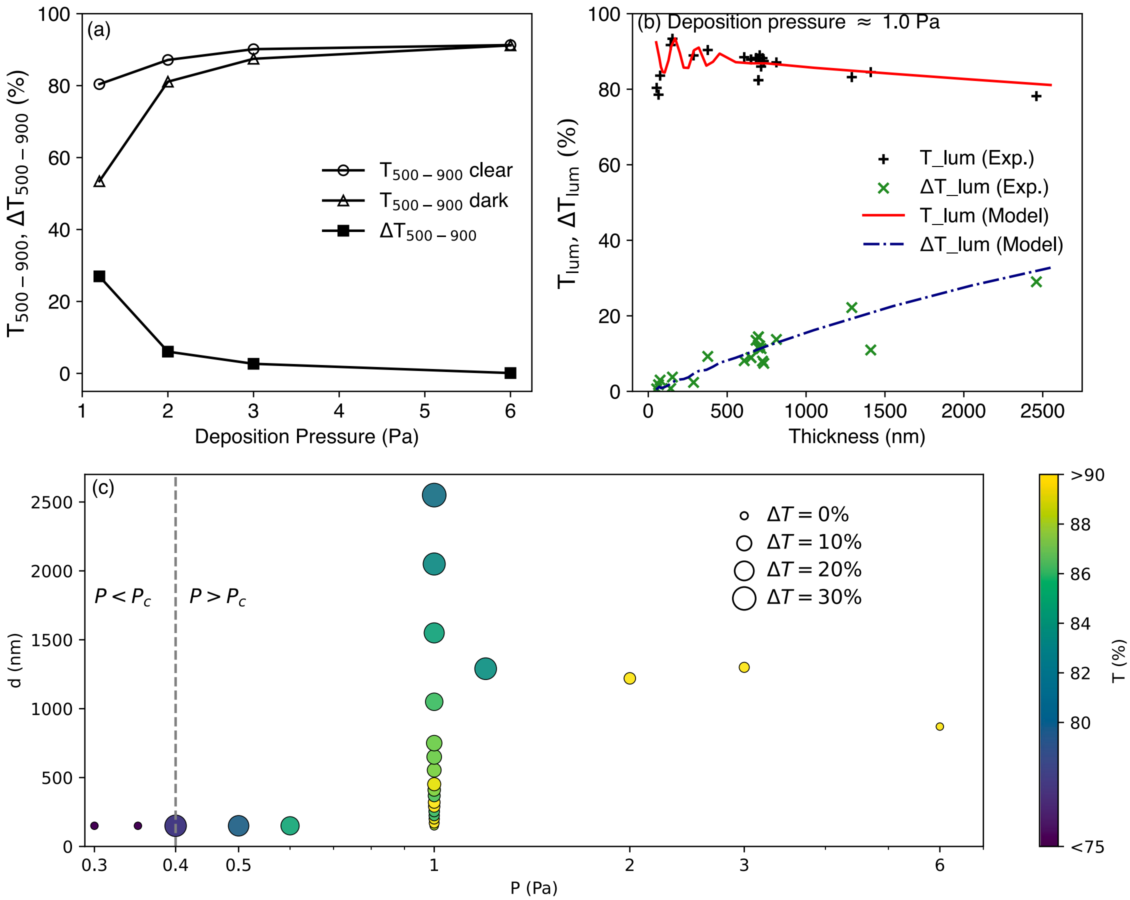

Fig. 7. Panel (a), shows T(λ) averaged between 500 and 900 nm, $T_{500\text{–}900}$, for the clear and dark state for YHO samples deposited at different deposition pressures. The change in $T_{500\text{–}900}$. i.e., $\Delta T_{500\text{–}900}$ after 1 h illumination with a solar simulator is also included. Panel (a) is reprinted from C.C. You et al. [79] with the permission of AIP Publishing. Panel (b) shows T_{lum} and ΔT_{lum} after 1 h solar simulator as a function of film thickness for samples synthesized at 1.0 Pa deposition pressure. Predicted values of T_{lum} and ΔT_{lum} according to the DMD model are also included. Panel (b) is reprinted from J. Montero and S. Zh. Karazhanov [61] with the permission of John Wiley & Sons, Inc. Panel (c) represents a map of the qualitative photochromic contrast ΔT and transparency T in the clear state of different YHO samples as a function of thickness d and deposition pressure P. The diameter of the circles is proportional to ΔT, whereas the color is proportional to T according to the color bar on the right. The figures in Panel (c) are not to be interpreted as absolute values but rather as representations to convey overall patterns of photochromic REHOs observed in the literature [44,61,79].

DMD model. Superimposed onto panel (b) are the results corresponding to the film prepared at 1.2 Pa by C. C. You et al. [79]. This particular film serves as a bridge between Refs. [61,79], since it was prepared using the same sputtering machine at approximately the same P and it was tested under the same illumination conditions.

According to Fig. 7(b), relatively thick films (above 2 μm) are required to achieve a good photochromic contrast $\Delta T_{lum} \sim 30\%$ at deposition pressures of 1.0 Pa. These films, despite their large thickness, are able to retain large transparency in the visible region, being $T_{lum\sim80\%}$. On the other hand, thinner films (d = 170 nm) prepared at 1.0 Pa exhibit higher transparency, $T_{lum\sim93\%}$, but very weak photochromic contrast, $\Delta T_{lum} \sim 3.0\%$. These results are consistent with the results reported by G. Colombi et al. [44] corresponding to 150 nm-thick YHO films deposited at 1.0 Pa. However, G. Colombi et al. [44] also demonstrated that 150 nm-thick YHO films deposited at lower pressures, closer to P_c, can exhibit transparency and photochromic contrast comparable to those achieved by ten times ticker films deposited at higher pressures [79].

As a summary of these observations, Fig. 7 panel (c) depicts a qualitative map of YHO films deposited at different pressures P and of different thicknesses d, which can convey the trend in transparency and contrast expected in other photochromic REHOs. In the graph, each point is represented by a circle, being the diameter of the circle proportional to the photochromic contrast and where the color of the circle represents the transparency in the clear state, according to the color scale in the figure. The critical pressure P_c is fixed at 0.4 Pa [35].

Numerical values, including pressure ranges, in Fig. 7 panel (c) are intended as an approximate guide for providing a general sense of the trends of transparency and photochromic contrast followed by REHOs, and must not be interpreted as absolute values. As it can be observed in Fig. 7 panel (c), samples with a larger photochromic modulation can be achieved either by *(i)* keeping a intermediate deposition pressure (e.g. 1.0 Pa) and increasing the film thickness above 1 μm or *(ii)*, by decreasing P towards P_c, and keeping the thickness of the films to few hundred nanometers. Obviously, samples deposited below P_c are neither photochromic nor transparent.

It is worth noting that photodarkened samples acquired following strategy *(ii)* present a much larger optical density in the photodarkened state that those obtained following *(i)*. On this basis, we can speculate that samples prepared by strategy *(i)*, which are more porous for being prepared higher pressures, contain a larger fraction of other phase or phases, e.g. an oxide phase not optically active. This idea agrees with previous studies that suggest that REHO photochromic films are indeed inhomogeneous, constituted by two [65] or more [96] coexisting phases. Moreover, this can be justified by the fitting to the DMD model: as it is observed Fig. 7(b), the change of transparency and photochromic contrast as a function of d follows very well the predictions of this model. For a correct fitting of the DMD model to the data presented in the figure, a thin Y_2O_3 layer (of constant thickness ∼ 50 nm) was assumed to form onto the surface of the film upon air exposure irrespective of the total film thickness [61]. For a fixed value of P, the presence of this layer, which is expected to be X-ray amorphous but its

Table 2
Luminous transmittance T_{lum}, and solar transmittance T_{sol} before (clear) and after (dark) illumination, as well as their respective change ΔT_{lum} and ΔT_{sol}, for Y, Gd, Dy, Er oxyhydrides. The thickness the samples are in the range 270 nm <d< 350 nm. The photodarkened state was measured after UV exposure during 5 h at a power 5070 μWcm^2. Data extracted from F. Nafezarefi et al. [35], see acknowledgments.

	T_{lum} (%)			T_{sol} (%)		
	Clear	Dark	ΔT_{lum}	Clear	Dark	ΔT_{sol}
YHO	79.9	50.1	29.8	77.6	53.5	24.1
GdHO	67	31.5	35.5	70.1	33.9	36.1
DyHO	59.8	37.2	22.6	58.1	36.3	21.7
ErHO	59.4	40.3	19.1	63.9	44.5	19.3

presence is confirmed by XPS [54], ion beam analysis [59] and neutron reflectometry [97], has an increasing impact on the optical properties of the samples as the total thickness is decreased. On this basis, by decreasing P, it is possible to obtain larger contrast in thinner layers, not only because the changes in stoichiometry of the oxyhydride phase itself derived from a lower incorporation of oxygen, but also because an increase in the oxyhydride/oxide ratio. This observation has also implications on the band gap determination: the presence of the oxide layer could lead to an overestimation of the band gap when calculated by optical methods.

3.3. Cation dependence

The transparency and photochromic contrast were studied for the first time for different RE cations by Nafezarefi et al. [35]. This preliminary study, which compares the photochromic effect of oxyhydrides of Y, Gd, Dy, and Er, provides T(λ) curves in the range 300 nm < λ < 2500 nm before and after illumination, which permits calculations of T_{lum}, T_{sol} as well as their change after illumination. The summary of these parameters is shown in Table 2. The data presented in Table 2 shows how samples with high transparency in the visible and solar spectra can provide large photochromic contrast, not only in the visible, but in the full solar range. Under the particular experimental conditions described in Ref. [35], oxyhydrides based on Y exhibit both the largest luminous transmittance and solar transmittance in the clear state (T_{lum} ~ 79.9%, T_{sol} ~ 77.6%). However, the largest photochromic contrast was achieved in Gd oxhydrides (ΔT_{lum} ~ 35.5%, ΔT_{sol} ~ 36.1%). Dy and Er oxyhydrides exhibited both lower transmittance and lower photochromic contrast.

Systematic studies on Y, Gd and Sc oxyhydrides [44], including variations in deposition pressure, controlled thickness and compositional analysis, pointed out to the possible connection between the cation ionic radius r_i and the photochromic contrast. According to this hypothesis, cations with a larger ionic radius (e.g. Gd^{3+}, r_i = 93.8 pm or Nd^{3+}, r_i = 98.3 pm), would result in oxyhydrides exhibiting a larger photochromic contrast than those formed by smaller cations, e.g. Y^{3+} (r_i = 90.0 pm), Sc^{3+} (r_i = 74.5 pm), Er^{3+} (r_i = 89.0 pm) or Dy^{3+} (r_i = 91.2 pm). This is partially confirmed by the study by S. M. Aðalsteinsson et al. [94] except for the case of Dy: in the later work, the thickness-normalized photochromic contrast from largest to smallest was found in DyHO, NdHO, GdHO and YHO thin films. Note: all the values of r_i provided in this section are sourced from the data compiled by R. D. Shannon [98].

However, this trend needs to be observed with caution because the deposition pressure and hence the oxygen content in the oxyhydride film have a tremendous effect in the photochromic effect. For a fair comparison, all different REHO films must be deposited at their own optimal conditions, and the illumination source must be chosen in accordance with the different optical absorption coefficients in order to avoid the influence of the *skin effect* (by which the proving beam will reach different depths in different samples depending on their optical band gap).

3.4. Excitation and recovery

Many organic photochromic compounds switch from a transparent state to a photodarkened state by the action of UV light [23]. Since usual soda lime glass absorbs most of the solar UV radiation, many photochromic compounds will not switch, or switch poorly when placed behind a glass pane. This is not the case of oxyhydrides: YHO has been found reactive to light from yellow (2.20 eV), green (2.34 eV), blue (2.80 eV) and to UV (3.14 eV and above) [99]. Not response has been observed under orange (1.94 eV) or red (1.80 eV) illumination [99]. In this particular case, the optical band gap of the studied YHO film was estimated to be ~ 2.39 eV.

The power of the light beam has also an influence in the photodarkening, where a higher power results in larger photochromic contrast. For similar power (e.g. yellow light at 4.9 mW/cm^{-2} and UV light at 5.1 mW/cm^{-2}) higher energetic light (UV) has been found to cause a larger photochromic contrast in YHO [99].

Given a fixed illumination wavelength and intensity, the temporal dependency of the photochromic contrast is observed to reasonably conform to a logarithmic law. In this sense, the largest photochromic contrast is achieved shortly after illumination has started: when illuminating YHO films with a solar simulator, there are not large differences in the photochromic contrast of samples illuminated during 5 h or 24 h [60].

Concerning the bleaching kinetics, the literature often relies on the time constant τ_b for evaluating how fast a photochromic material bleaches back to the original state once illumination has ceased [44, 100]. τ_b can be calculated according to:

$$\ln\left(-\ln\frac{\langle T(t)\rangle}{\langle T_{clear}\rangle}\right) = -\frac{1}{\tau_b}t - \ln(\langle T_{dark}\rangle) \quad (5)$$

where $\langle T(t)\rangle$ is the average transmittance in a certain wavelength range (e.g. 450 nm < λ < 1000 nm) as a function of illumination time t, and $\langle T_{clear}\rangle$ and $\langle T_{dark}\rangle$ are the average transmittance in the aforementioned wavelength range in the clear (initial or clear) and photodarkened (final) state. Eq. (5) assumes that the species responsible of the photodarkening of the film decrease as a function of time following first order kinetics [100].

Once again, τ_b depends on the deposition pressure, being smaller (i.e., faster bleaching) at deposition pressures far from P_c, where transparency is high but photochromic contrast is low. Also, the ionic radius seems to play a role, where smaller cations (Sc) result in longer bleaching times that larger cations (Y, Gd). According to the literature [44], it is possible to achieve YHO and GdHO films exhibiting excellent transparency, photochromic contrast and bleaching speed: $T_{450-1000}$ ~ 84, 83%, $\Delta T_{450-1000}$ ~ 18, 20%, τ_b = 12, 9 min for YHO and GdHO respectively. These data correspond to 150 nm-thick films illuminated with UV light (385 nm, power 75 mW/cm^2) during 30 min.

In addition, the temperature of the sample has an effect on the photochromic contrast and darkening/bleaching speed [44]. Under illumination, photodarkening and thermal bleaching compete, reaching an equilibrium. This equilibrium is altered by the temperature of the film. R. Hallaråker et al. [101] investigated the effect that the temperature (in the range between 37 °C and 87 °C) has on the photochromic contrast of YHO films. For a fixed wavelength and power of the illumination source, the higher the temperature at which the photochromic YHO film is kept, the lower the final photochromic contrast achieved. Besides, in the absence of illumination, photodarkened YHO films kept at higher temperatures recovered faster than those at lower temperatures.

A photochromic REHO film will heat up under real solar illumination because it becomes optically absorbing when photodarkened. In this sense, the photochromic contrast may be lower than that achieved when the film is illuminated with an LED source. The reverse is also true as reported by E. M. Baba et al. [102]: an YHO film, when cooled down to ~ −268 °C (5 K), is able to achieve a larger photochromic contrast than an equivalent film kept at room temperature [102]. According to this study, partial bleaching occurs in temperatures ranging from −173 °C (100 K) to −23 °C (250 K) [102].

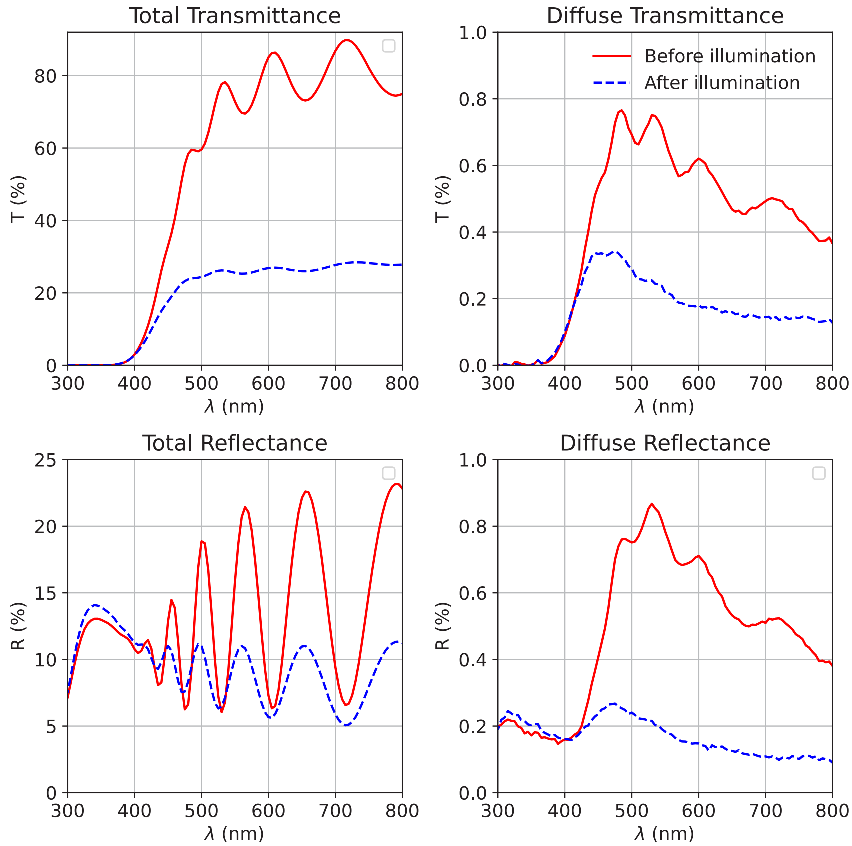

Fig. 8. Total transmittance (top left), diffuse transmittance (top right), total reflectance (bottom left) and diffuse transmittance (bottom right) of a YHO film (ca. 1 μm thick) before and after UV illumination (365 nm). The measurements where performed in a Perkin-Elmer Lambda-900 spectrophotometer equipped with an integrating sphere. Measured at normal incidence.

3.5. Haze and color perception

Receiving natural light and allowing visual contact with the exterior stands as a primary and fundamental goal in architectural glazing. This involves the creation of occupant-friendly well-illuminated spaces by making the most out of natural daylight, while at the same time offering the occupants the possibility to engage visually with the external surroundings [11]. These aspects have been proven to have a positive effect in the recovery of patients in hospitals [103], make employees more productive [104], improve academic performance of students [105] and, although this is a bold statement difficult to quantify, make our daily life more pleasant.

On this basis, current architectural trends highlight the importance of a multidimensional combination of several factors including the well-being of the occupants, aesthetics and the efficient use of energy resources. This is not without a purpose: we spend up to 90% of our times indoors [106]!

As we have discussed previously, in the context of daylight management, we expect $T(\lambda)$ in the visible region to be as large as possible in the clear state, while at the same time keeping a large photochromic response. In this way we can ensure natural light and visual comfort by preventing glare. As we have seen, this information can be reduced to T_{lum} and ΔT_{lum}. Besides, except for specific applications involving privacy or solar control by light back-scattering [107], we want glazing to scatter light as little as possible to ensure a clear view.

In this section we will study the scattering properties as well as color neutrality aspects in photochromic oxyhydrides. After all, glazing act as an optical filter through which we see the exterior and receive light. On this basis, we have to assess the quality of the visual connection with the ambience and the quality of the light that we receive through REHO-coated glasses. Color perception is a subjective experience and often requires the conduction of perception surveys amongst users [108,109].

Light scattering, caused e.g. by particulate-films [110] or surface roughness [111] (i.e., Mie scattering), can result in films exhibiting a turbid or *milky* appearance which can severely limit the visibility through them. This effect is manifested by large values of diffuse transmittance or reflectance. Fig. 8 shows the total transmittance and reflectance (left, top and bottom panels respectively), corresponding to an YHO film before and after UV illumination, as measured in a Perkin-Elemer Lambda 900 spectrophotometer equipped with an integrating sphere. Total transmittance (or reflectance) values are important because they represent the fraction of light that is transmitted (or reflected) considering both, direct and scattered light. As mentioned before, since both total transmittance and reflectance decrease after illumination, and according to Eq. (4), the film becomes absorbing after illumination, with the implications already discussed above. Measurements of diffuse transmittance and reflectance (Fig. 8, right top and bottom panels), revealed that the fraction of light that suffers scattering is very low, below 1.0% in the clear state and even lower in the dark state. As a comparison, in thermotropic hydrogels, which provide dynamic solar control by varying their light scattering properties in the backward direction [107,112], the fraction of scattered light can reach values > 80 %, where visibility is severely impaired [113]. In contrast, the low values observed in YHO guarantee a clean view without haze in both clear and photodarkened state.

On the other hand, large values of T_{lum} and lack of scattering are not always synonym of color neutrality. In fact, REHOs are often described as *yellowish* [34,40,42,99,108]. In this sense S. Arbab et al. [108] studied how different colors, under different illumination conditions, are perceived when observed through an YHO-coated photochromic glass pane. For this purpose, 21 participants were asked to undergo

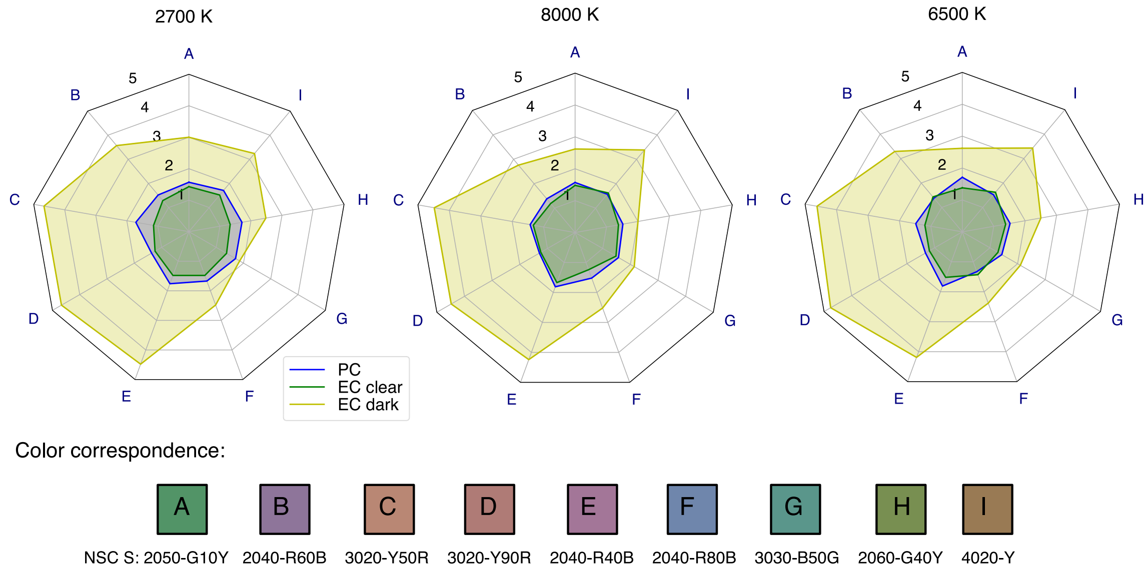

Fig. 9. Perception of nine different colors through two types of glass: electrochromic in the clear and dark state (EC clear, EC dark) and photochromic YHO (PC). Each case was studied under three illumination conditions corresponding to light of correlated color temperature of 2700 K (left panel), 8000 K (center panel), 6500 (right panel). Results are presented in three radar charts (one for each illumination temperature) of 9 spikes, where each spike corresponds to a particular color, labeled with letters from *A* to *I*. The correspondence of these labels with their respective color is depicted in NCS notation (bottom panel) together with a square of approximate color as reference. The radial direction, starting from the center of the radar chart and moving outwards, correspond to the average score given to each particular color (1 corresponds to a perfect match with the reference color, whereas 5 corresponds to a large deviation in the color perception).
Source: Adapted from the work of S. Arbab et al. [108] (CC-BY)

a matching procedure in which a panel containing an arrangement of rectangles of 9 different colors was observed through an YHO coated glass. An identical reference panel was simultaneously available without any, coated or otherwise, glass plane obstructing the view. The panels contained colors corresponding to the NCS codes as shown in Fig. 9 (bottom), where they have been labeled from letters *A* to *I* for convenience. Additionally, in Fig. 9 bottom panel, a square with an approximate visual representation of each color is presented. Participants were told to evaluate (by giving a score from 1 to 5, were 1 is a perfect agreement with the color in the reference panel) how they perceived each color through the YHO coated glass.

The experiment was performed under different illumination temperatures: 2700 K (corresponding to sunrise or sunset), 8000 K (corresponding to midday clear sky illumination) and 6500 K (corresponding with midday overcast sky). The average scores given by the participants for each color and for the YHO glass (clear state), together with those corresponding to an analogous experiment using electrochromic glass (manufactured by Gesimat) in the clear and dark state, are compiled in the radar charts in Fig. 9 left panel (2700 K), middle panel (8000 K), and right panel (6500 K).

As it can be observed in Fig. 9, the electrochromic window and the photochromic YHO glass pane (both in the clear state), have very little effect in the perception of the different colors, with scores between 1 and 2 irrespective of the illumination conditions. This is a surprise for the *yellowish* YHO film. In the dark state, however, the electrochromic film has a profound effect in the colors close to the red spectrum, namely C (NCS S 3020-Y50R, light yellowish red), D (NCS S 3020-Y90R, light greyish red) and E (NCS S 2040-R40B, light reddish purple). It is worth noting that the typical electrochromic device manufactured by Gesimat, include a Prussian blue layer as ion storage layer [29], which provides a large absorption in longer wavelengths of the visible spectrum in the dark state, hence the large distortion on the perception of reddish colors observed in Fig. 9. Unfortunately no data were presented regarding the YHO film in the photodarkened state. However, since the decrease in transmittance in the photodarkened state occurs evenly in the visible spectrum, see e.g. Fig. 6 (left column top), we can speculate that color neutrality is also expected in the dark state.

In contrast, follow up studies by S. Arbab et al. [109] demonstrated that the hue perception of yellow, red and violet colors was largely affected when seen by light that has passed through an YHO-coated glass pane. Unfortunately, Arbab et al. [108,109] do not provide any information about the nature of the YHO coating, e.g. deposition pressure, thickness, T_{lum}, T_{sol} or comment on the photodarkened state. In any case, the takeout message is clear: the color neutrality of REHOs needs to be improved for a satisfactory application in glazing.

3.6. Durability

In contrast to organic materials, REHOs are not expected to degrade by UV light, and hence UV-dosage test, commonly applied in the organic photochromic industry, may not be the most adequate in this case [23]. In this sense, adequate durability tests for REHOs need to be devised, and presumably will involve repeatedly photochromic switching. Unfortunately, studies involving durability tests of any kind, performed on these materials, are lacking in the literature. However, as discussed below, it is already possible to identify some vulnerabilities of REHOs.

As observed in Table 1, REHOs seem to gradually incorporate oxygen from the atmosphere and lose hydrogen [43,70,79,114]. As discussed before, there is an optimal O/RE ratio at which a maximum photochromic contrast is achieved combined with a reasonable transparency in the clear state and bleaching kinetics. The gradual incorporation of oxygen by air exposure result in a weakened photochromic response. Besides, the incorporation of oxygen causes a lattice expansion as observed by X-ray diffraction [43,44,70]. This expansion may be the source of lattice strain and delamination. In fact, in our experience, films kept in air tend to suffer from flaking and delamination after a period of time that can vary from few days, in the case of NdHO [43] to years in the case of YHO. Fig. 10 left panel shows a photomicrograph of a YHO film after storage during ca. 4 years in air. Different regions of the film show different degrees of delamination.

In principle, ageing by oxidation can be avoided by lamination or capping of the photochromic film [43]. However, as we have demonstrated [54], correct bleaching requires, at least under certain conditions of illumination power and wavelength, the availability of oxygen

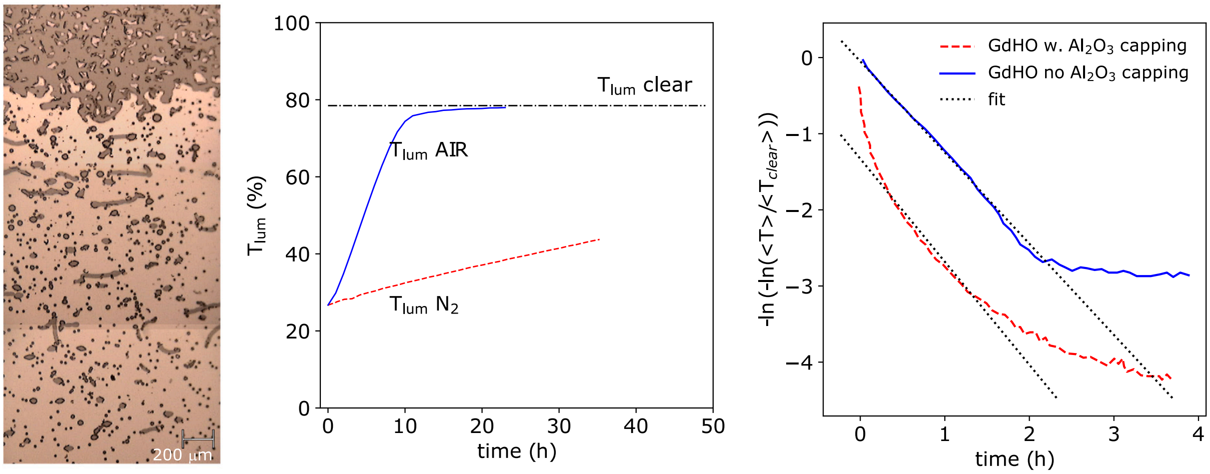

Fig. 10. Left panel: photomicrograph showing the delamination observed in a YHO film after ca. 4 years of storage in air, courtesy of Senior Research Engineer J. Thyr. Middle panel: evolution of T_{lum} of a photodarkened YHO film during bleaching in air or N_2 atmosphere. The horizontal dashed line indicates the value of T_{lum} in the clear state. Adapted from our previous work [54] (CC-BY). Right panel: bleaching of a GdHO photodarkened film with and without Al_2O_3 capping plotted in a double logarithm plot according Eq. (5). ⟨T⟩ stands for the average transmittance between 450 and 1000 nm. Dashed black lines correspond to the slope calculated following this model.
Source: Adapted from Ref. [43] (CC-BY).

in the surrounding environment [54,115,116]. Fig. 10 middle panel, depicts the evolution of T_{lum} corresponding to a photodarkened YHO coating as it bleaches in air or in nitrogen atmosphere [54]. As it can be observed, the film recovers much faster in air than in an inert atmosphere. We note that the fact that the film was photodarkened by *repeatedly* cycling is relevant: the recovery of the sample decreased gradually as it was subjected to illumination/darkness cycles in nitrogen [54]. This need to be considered when implementing REHOs in glazing: a common strategy for controlling heat transfer by conduction include the use of multiple glass panes in between which inert gas (e.g. Ar) is confined [82,117]. It is not clear how placing REHO coatings facing this confined spaces can affect the bleaching kinetics of the photodarkened films.

Environmental dependence

The environmental dependence of the bleaching effect in YHO films shown in Fig. 10 has a strong resemblance with the photochromic behavior in transition metal oxides such as WO_3 [118,119] or related compounds [120], in which oxygen plays an important role. In particular, C. Bechinger et al. [118] identified two different channels in the bleaching kinetics of photodarkened WO_3, one associated to interstitial oxygen and a second one associated to ambient oxygen, which bears similarities with our data presented in Fig. 10 middle panel.

YHO films protected by Al_2O_3 and Si_3N_4 coatings deposited by sputtering retain unaltered the reversibility according to previous works [121]. These capping layers, which were 50 (Al_2O_3) and 60 nm (Si_3N_4) thick, were prepared without intentional substrate heating under relatively high (0.8 Pa for Si_3N_4) and very high (5.0 Pa for Al_2O_3) deposition pressures. However, as discussed previously and as described by the Thornton diagram [62], Fig. 5 panel (a), films deposited at high pressure and low temperature may not be optimal as oxygen-diffusion barriers.

In contrast, coatings deposited by atomic layer deposition ALD, may be more compact and able to prevent oxidation. Studies on photochromic NdHO revealed that these films, when encapsulated by ALD-deposited Al_2O_3 capping layers (47 nm thick), were able to photodarken normally under illumination, but the change in the reversibility kinetics was noticeable [43]. The capping, however, helped in stabilizing the NdHO coatings, which otherwise detached from the substrate after few minutes in air.

The recovery kinetics of Al_2O_3 photochromic GdHO films is severely impacted by encapsulation in a way that the assumption of a first-order process described by Eq. (5) is no longer valid [43]. As observed in Fig. 10 right panel, only uncapped GdHO follows first-order kinetics according to Eq. (5). This is attributed to the effect of the capping layer itself, as well as to the removal of defects due to the relatively-high temperature (87 °C) achieved during the ALD process by which the Al_2O_3 capping was deposited on top of the GdHO film. These observations lead us to the next point: how stable are REHOs when subjected to relatively high temperatures (up to 100 °C)?

Thermal stability

YHO films can withstand annealing at temperatures ~ 100 °C in air during 30 min, without suffering a substantial impact on their transparency and photochromic contrast [90,99]. R. Hallaråker et al. [101] reported that heating YHO films at 87 °C in air do not prevent the films from fully bleaching to their original state. YHO samples annealed above ~ 100 °C incorporated oxygen while at the same time released hydrogen [90,99], leading to an increased transparency in the clear state, but to a reduced, or even suppressed, photochromic contrast [99]. Of course, the thermal stability may depend on the cation of the REHO film but these preliminary studies suggest that photochromic REHOs can withstand the typical temperatures that glazing can reach in sunny days without problems.

Summary and outlook

Rare earth oxyhydrides (REHOs), with RE = Y, Gd, Dy, Er, Sm, Nd, Sc, are photochromic materials exhibiting many attractive features for their application in large-area transmittance control applications. REHOs present high transmittance in the visible region, while a large (and rapid) photochromic transmittance switching, particularly homogeneous in the visible range, occurs across the full solar spectrum range. The photochromic effect can be triggered by light in the visible region, without needing UV. REHOs are materials rather resilient to temperature and can be prepared by readily scalable methods for the glazing industry. Based on the study of existing literature, no other family of photochromic materials is able to combine all these desirable properties.

REHOs can be fabricated by magnetron sputtering, a technique frequently used by the glazing industry, and are inorganic thus, in principle, more stable than organic dyes. During the sputtering process, the deposition pressure is a crucial parameter that dictates how permeable the coatings are to oxygen, ultimately influencing their transparency,

Table 3
Frequently asked questions and answers when it comes to the implementation of rare earth oxyhydrides for solar control transmittance in glazing.

Question	Answer
Can REHOs be prepared onto large substrates?	REHOs can be prepared by magnetron sputtering, a technique that is compatible with large area fabrication. The process takes place without intentional substrate heating and hence allows the use flexible substrates and roll-to-roll fabrication.
Does the photodarkening only occur by the action of UV light?	No, they darken with less energetic light as well, e.g. YHO even switches by the effect of ~ 2.2 eV light. Of course, there is a dependency on light power and energy: intense light sources of shorter wavelengths result in larger photochromic contrast that less intense and energetic light.
In which wavelength range the optical switching occur?	The switching occurs from 300 nm to 2500 nm and beyond, covering both the visible part of the spectrum and the solar spectrum. The switching occur fairly evenly in this wavelength range.
Is the photochromic contrast in the transmittance caused by an increase of reflection or absorption?	Under illumination REHOs switch from light transparent to light absorbing. For this reason, the temperature of the coating is expected to strongly increase under solar light. As a consequence, REHOs need to be used in combination with low-E coatings to prevent re-radiated heat to penetrate the building. Also, as with electrochromic coatings, when implemented onto glass substrates, tempered glass may be required to withstand the temperature changes that may occur during operation.
What are typical values of T_{lum} and ΔT_{lum} ?	For YHO samples exhibiting $T_{lum} \sim 80\%$ it is possible to achieve $\Delta T_{lum} \sim 30\%$ after 1 h illumination with a solar simulator. This values may vary depending on illumination time and temperature.
What are typical values of T_{sol} and ΔT_{sol} ?	There are not many reports that include a wide-enough wavelength range (optical measurements are typically restricted to the UV–VIS region) to calculate this parameters. We have reported T_{sol}= 65% and ΔT_{sol}= 50% in GdHO films after 15 h illumination with 365 nm-led light. To our knowledge, measurements of T_{sol} and ΔT_{sol} under real or simulated solar conditions are lacking in the literature.
Are REHOs in the transparent state color-neutral?	REHOs usually present a yellowish appearance. However, color perception surveys revealed that the perception of colors does not vary significantly when seen through an YHO-coated glass pane. However, light passing through an YHO-coated glass pane can impact hue perception of yellow, red and violet colors.
Can a clear film become dark by the effect of light even if the temperature is high?	Under illumination, darkening/bleaching processes compete, thus, for a fixed intensity, the higher the temperature the smaller the switching. However, the capacity of switching in YHO has been demonstrated at temperatures as high as ~ 90 °C.
Can a photodarkened film bleach back to the transparent state during cold weather?	The bleaching is a thermal process that is severely affected by temperature. However, it has been demonstrated that some partial bleaching can occur in YHO even at temperatures below 100 K. To our knowledge, experiments under realistic of REHO-glazing operating during winter have not been reported.
How durable are REHOs?	As inorganic materials, REHOs are not expected to degrade by the action of UV light. However, it has been observed that, when kept in air, they tend to incorporate oxygen and release hydrogen, reducing for this reason their photochromic performance. The incorporation of oxygen causes the expansion of the crystalline lattice, causing strain between the film and the substrate, which can lead to delamination.
In an insulating glass unit IGU, is it possible to place the photochromic coating facing the space between two glass panes?	This issue can be problematic, since the space between glass panes in a IGU is typically filled with Ar or other gasses to reduce thermal conduction and the bleaching of YHO has been proven to be dependent on the environment. Photodarkened films kept in oxygen-free atmosphere tend to bleach slower than those kept in air. However, it is worth noting that the gas filling between window panes is not completely oxygen-free.
Can REHOs be protected from the environment by lamination of capping?	This is a controversial topic. Given the previous point, it is expected from lamination to affect the bleaching of REHO coatings. ALD-deposited Al_2O_3 onto Gd_2O_3 has been found affect the recovery kinetics. On the other hand sputtered Si_3N_4 or Al_3O_3 capping layers prepared in Zone 1 of Thornton diagram have been reported to allow the recovery of YHO films.

photochromic contrast and bleaching/darkening kinetics. The selection of the RE cation has a impact on these parameters as well: in principle, cations of large ionic radii result in photochromic films exhibiting faster bleaching and largest contrast, but at the cost of a reduced transparency in the clear state.

The application of REHOs in the glazing industry is not without challenges, strategies for achieving long-term stability without imperiling photochromic contrast and dynamics must be devised. In Table 3 we discuss some of the most pressing issues when it comes to the implementation in glazing of REHOs.

Provided that these challenges are met, REHOs can be the key to photochromic smart glazing, regulating solar transmittance on demand to enhance thermal and visual comfort for building occupants, while reducing energy consumption. During hot sunny days, a REHO-based coating can remain dark, limiting the inlet of solar energy and solar light to the building, reducing the cooling load and preventing glare. On dark cold days, the coating can remain transparent, providing as much daylight as possible and ensuring an unobstructed visual contact with the surroundings. Note that while the laboratory photochromic performance of REHOs is very promising, it is essential to validate the results in real-world applications. Factors such as illumination, temperature, and other environmental conditions may significantly impact the photochromic switching and dynamics.

A word on materials sustainability

Rare earth metals, which constitute the base of this photochromic technology, are much more abundant in the Earth's crust than Ag or In, and have a similar (although still higher) abundance than that of Sn or

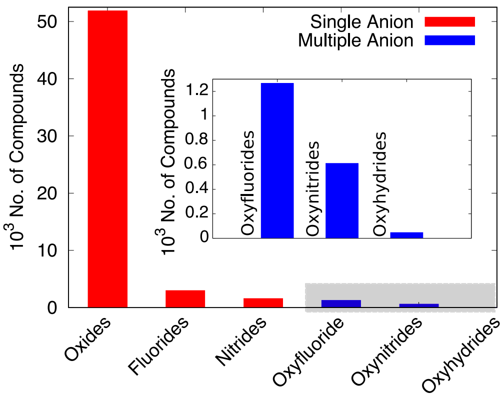

Fig. 11. Number of reported inorganic compounds including single anion (oxides, fluorides, nitrides) and mixed anion (oxyfluorides, oxynitrides and oxyhydrides). The insert is a magnification of the shadowed area in the main graph.
Source: Adapted from H. Kageyama et al. [41](CC-BY).

W [122]. We note that Ag, In, Sn, and W, are commonly used today in commercial glazing [11]. Unfortunately, the use of rare earths comes with supply bottlenecks, geopolitical aspects and sustainability issues that, although out of the scope of this work, need to be addressed carefully when it comes to a practical application [123]. Fortunately, we can benefit from the emerging models and strategies by the permanent magnet industry, in which rare earth metals play a fundamental role, towards a clean and sustainable supply of these metals [123–125].

Oxyhydrides: a terra ignota

The development of photochromism in oxyhydrides illustrates the possibilities that can arise from the exploration of mixed anion compounds as recently highlighted by H. Kageyama et al. [41]. This new form of chemistry could potentially offer the possibility to obtain functional materials with properties previously beyond reach, for example, in the case in question, the synthesis of photochromic materials by methods compatible with large-area fabrication. While inorganic functional materials based on single anion compounds have been extensively investigated for decades, multiple anion compounds are a true *terra ignota* [41,126]. Indeed, as shown in Fig. 11, the number of reported inorganic single anion compounds, including oxides, fluorides and nitrides, is overwhelmingly larger than the number of reported inorganic mixed anion compounds (e.g. oxyfluorides, oxynitrides and oxyhydrides). The lack of knowledge in the field of mixed anion compounds is daunting, especially in the case of oxyhydrides (see inset in Fig. 11). The huge technological potential of oxyhydrides remains largely unexplored [126].

CRediT authorship contribution statement

José Montero-Amenedo: Writing – review & editing, Writing – original draft, Visualization, Validation, Investigation, Funding acquisition, Formal analysis, Conceptualization.

Declaration of competing interest

The authors declare that they have no known competing financial interests or personal relationships that could have appeared to influence the work reported in this paper.

Acknowledgments

This work has been supported by the Swedish Energy Agency E2B2 Project Ref. P2022-00859. The author is grateful to Em. Prof. Dr. B. Dam for the help in verifying the values presented in Table 2, and to Prof. Dr. S. Zh. Karazhanov and Dr. T. Mongstad for the fruitful discussions over the years.

References

[1] C.M. Lampert, C.G. Granqvist, Large-area chromogenics: Materials and devices for transmittance control, in: Society of Photo-Optical Instrumentation Engineers (SPIE) Conference Series, vol. 10304, 1990.
[2] C.G. Granqvist, Chromogenic materials for transmittance control of large-area windows, Crit. Rev. Solid State Mater. Sci. 16 (5) (1990) 291–308, http://dx.doi.org/10.1080/10408439008242184.
[3] J.S.E.M. Svensson, C.G. Granqvist, Electrochromic coatings for smart windows: Crystalline and amorphous WO_3 films, Thin Solid Films 126 (1–2) (1985) 31–36, http://dx.doi.org/10.1016/0040-6090(85)90171-3.
[4] C.M. Lampert, Electrochromic materials and devices for energy efficient windows, Sol. Energy Mater. 11 (1) (1984) 1–27, http://dx.doi.org/10.1016/0165-1633(84)90024-8.
[5] C. Granqvist, S. Green, G. Niklasson, N. Mlyuka, S. von Kræmer, P. Georén, Advances in chromogenic materials and devices, Thin Solid Films 518 (11) (2010) 3046–3053, http://dx.doi.org/10.1016/j.tsf.2009.08.058.
[6] International Energy Agency, Report: Tracking clean energy progress, 2023, URL https://www.iea.org/reports/tracking-clean-energy-progress-2023. (Accessed on 29 April 2024).
[7] European Commission, Smart windows: A no-brainer for future buildings, 2023, Online. URL https://cordis.europa.eu/article/id/400002-smart-windows. (Accessed on 29 April 2024).
[8] B. Richter, D. Goldston, G. Crabtree, L. Glicksman, D. Goldstein, D. Greene, D. Kammen, M. Levine, M. Lubell, M. Savitz, D. Sperling, F. Schlachter, J. Scofield, J. Dawson, How America can look within to achieve energy security and reduce global warming, Rev. Mod. Phys. 80 (2008) S1–S109, http://dx.doi.org/10.1103/RevModPhys.80.S1.
[9] C.G. Granqvist, İ.B. Pehlivan, G.A. Niklasson, Electrochromics on a roll: Web-coating and lamination for smart windows, Surf. Coat. Technol. 336 (2018) 133–138, http://dx.doi.org/10.1016/j.surfcoat.2017.08.006.
[10] J. Montero, Electro- and photochromic oxide-related materials and applications, in: Sustainable Nanomaterials for Energy Applications, in: 2053-2563, IOP Publishing, Bristol (UK), 2023, pp. 8–1–8–28, http://dx.doi.org/10.1088/978-0-7503-3531-7ch8.
[11] G.B. Smith, C.G. Granqvist, Green Nanotechnology: Solutions for Sustainability and Energy in the Built Environment, CRC Press, Boca Raton, 2010, http://dx.doi.org/10.1201/EBK1420085327.
[12] S. Bhattacharjee, S. Lidelöw, F. Shadram, Energy and indoor thermal performance analysis of a glazed façade high-rise building under various nordic climatic conditions, Energy Rep. 10 (2023) 3039–3053, http://dx.doi.org/10.1016/j.egyr.2023.09.090.
[13] A. Cannavale, U. Ayr, F. Fiorito, F. Martellotta, Smart electrochromic windows to enhance building energy efficiency and visual comfort, Energies 13 (6) (2020) 1449, http://dx.doi.org/10.3390/en13061449.
[14] A. Azens, C.G. Granqvist, Electrochromic smart windows: Energy efficiency and device aspects, J. Solid State Electrochem. 7 (2003) 64–68, http://dx.doi.org/10.1007/s10008-002-0313-4.
[15] A. Piccolo, Thermal performance of an electrochromic smart window tested in an environmental test cell, Energy Build. 42 (9) (2010) 1409–1417, http://dx.doi.org/10.1016/j.enbuild.2010.03.010.
[16] A. Jonsson, A. Roos, Evaluation of control strategies for different smart window combinations using computer simulations, Sol. Energy 84 (1) (2010) 1–9, http://dx.doi.org/10.1016/j.solener.2009.10.021.
[17] N.L. Sbar, L. Podbelski, H.M. Yang, B. Pease, Electrochromic dynamic windows for office buildings, Int. J. Sustain. Built Environ. 1 (1) (2012) 125–139, http://dx.doi.org/10.1016/j.ijsbe.2012.09.001.
[18] P.F. Tavares, A.R. Gaspar, A.G. Martins, F. Frontini, Evaluation of electrochromic windows impact on the energy performance of buildings in mediterranean climates, Energy Policy 67 (2014) 68–81, http://dx.doi.org/10.1016/j.enpol.2013.07.038.
[19] A. Piccolo, C. Marino, A. Nucara, M. Pietrafesa, Energy performance of an electrochromic switchable glazing: Experimental and computational assessments, Energy Build. 165 (2018) 390–398, http://dx.doi.org/10.1016/j.enbuild.2017.12.049.
[20] A. Cannavale, F. Martellotta, P. Cossari, G. Gigli, U. Ayr, Energy savings due to building integration of innovative solid-state electrochromic devices, Appl. Energy 225 (2018) 975–985, http://dx.doi.org/10.1016/j.apenergy.2018.05.034.
[21] R. Tallberg, B.P. Jelle, R. Loonen, T. G., M. Hamdy, Comparison of the energy saving potential of adaptive and controllable smart windows: A state-of-the-art review and simulation studies of thermochromic, photochromic, and electrochromic technologies, Sol. Energy Mater. Sol. Cells 200 (2019) 109828, http://dx.doi.org/10.1016/j.solmat.2019.02.041.
[22] W. Armistead, S. Stookey, Photochromic silicate glasses sensitized by silver halides: Their characteristic of changing color reversibly, in combination with other properties, suggests many uses, Science 144 (3615) (1964) 150–154, http://dx.doi.org/10.1126/science.144.3615.150.
[23] A.D. Towns, Applied photochemistry, in: G.B.A.S. Silvi (Ed.), Springer, Chem, 2016, pp. 227–279, http://dx.doi.org/10.1007/978-3-319-31671-0.

[24] M. Luo (Ed.), Encyclopedia of Color Science and Technology, Springer Science+Business Media New York, 2016, http://dx.doi.org/10.1007/978-1-4419-8071-7.

[25] R.J. Araujo, Photochromic glasses, in: R.A. Meyers (Ed.), Encyclopedia of Physical Science and Technology (Third Edition), third ed., Academic Press, New York, 2003, pp. 49–56, http://dx.doi.org/10.1016/B0-12-227410-5/00567-6.

[26] K.A. Landa, L.M. Landa, A.V. Longobardo, S. Thomsen, Photochromic float glasses and methods of making the same, 2004, United States Patent No. US 6711917B2.

[27] K. Fries, C. Fink-Straube, M. Mennig, H. Schmidt, Sol-gel technologies for glass producers and users, in: M. Mennig, M.A. Aegerter (Eds.), Sol-Gel Technologies for Glass Producers and Users, Springer US, 2004, Ch. Photochromic Coatings.

[28] B.V. Gemert, The commercialization of plastic photochromic lenses: A tribute to John Crano, Mol. Cryst. Liq. Cryst. Sci. Technol. 344 (2000) 57–62, http://dx.doi.org/10.1080/10587250008023814.

[29] M. Ferrara, M. Bengisu, Materials that Change Color, 2014, https://doi-org.ezproxy.its.uu.se/10.1007/978-3-319-00290-3.

[30] M. Bourdin, G. Salek, A. Fargues, S. Messaddeq, Y. Messaddeq, T. Cardinal, M. Gaudon, Investigation on the coloring and bleaching processes of WO_{3-x} photochromic thin films, J. Mater. Chem. C 8 (2020) 9410–9421, http://dx.doi.org/10.1039/D0TC02170A.

[31] J. Chen, A.W.M. Tan, A.L.-S. Eh, P.S. Lee, Scalable inkjet printing of electrochromic smart windows for building energy modulation, Adv. Energy Sustain. Res. 3 (5) (2022) 2100172, http://dx.doi.org/10.1002/aesr.202100172.

[32] J.-H. Kim, S.-H. Han, Indoor daylight performances of optimized transmittances with electrochromic-applied kinetic louvers, Buildings 12 (3) (2022) 263, http://dx.doi.org/10.3390/buildings12030263.

[33] C.G. Granqvist, Handbook of Inorganic Electrochromic Materials, Elsevier Science, 1995, http://dx.doi.org/10.1016/B978-0-444-89930-9.X5000-4.

[34] T. Mongstad, C. Platzer-Björkman, J.P. Maehlen, L.P. Mooij, Y. Pivak, B. Dam, E.S. Marstein, B.C. Hauback, S.Z. Karazhanov, A new thin film photochromic material: Oxygen-containing yttrium hydride, Sol. Energy Mater. Sol. Cells 95 (12) (2011) 3596–3599.

[35] F. Nafezarefi, H. Schreuders, B. Dam, S. Cornelius, Photochromism of rare-earth metal-oxy-hydrides, Appl. Phys. Lett. 111 (10) (2017) 103903, http://dx.doi.org/10.1063/1.4995081.

[36] J. Montero, F.A. Martinsen, M. Lelis, S.Z. Karazhanov, B.C. Hauback, E.S. Marstein, Preparation of yttrium hydride-based photochromic films by reactive magnetron sputtering, Sol. Energy Mater. Sol. Cells 177 (2018) 106–109, http://dx.doi.org/10.1016/j.solmat.2017.02.001, Note: preprint published in arXiv:1610.08263 (2016).

[37] H. Gläser, Large Area Glass Coating, Von Ardenne Anlagen Technik, 2000.

[38] G.G. Libowitz, A.J. Maeland, Hydrides, in: Handbook on the Physics and Chemistry of Rare Earths, vol. 3, Elsevier Science, North-Holland, 1979, pp. 299–336, Ch. 26.

[39] S. Zhang, R. Xiao, Yttrium oxide films prepared by pulsed laser deposition, J. Appl. Phys. 83 (1998) 3842–3848, http://dx.doi.org/10.1063/1.366615.

[40] S. Cornelius, G. Colombi, F. Nafezarefi, H. Schreuders, R. Heller, F. Munnik, B. Dam, Oxyhydride nature of rare-earth-based photochromic thin films, J. Phys. Chem. Lett. 10 (6) (2019) 1342–1348, http://dx.doi.org/10.1021/acs.jpclett.9b00088.

[41] H. Kageyama, K. Hayashi, K. Maeda, J.P. Attfield, Z. Hiroi, J.M. Rondinelli, K.R. Poeppelmeier, Expanding frontiers in materials chemistry and physics with multiple anions, Nature Commun. 9 (1) (2018) 1–15, http://dx.doi.org/10.1038/s41467-018-02838-4.

[42] D. Chaykina, G. Colombi, H. Schreuders, B. Dam, Photochromic samarium oxyhydride thin films, AIP Adv. 13 (5) (2023) 055211, http://dx.doi.org/10.1063/5.0147423.

[43] D. Chaykina, F. Nafezarefi, G. Colombi, S. Cornelius, L.J. Bannenberg, H. Schreuders, B. Dam, Influence of crystal structure, encapsulation, and annealing on photochromism in nd oxyhydride thin films, J. Phys. Chem. C 126 (4) (2022) 2276–2284, http://dx.doi.org/10.1021/acs.jpcc.1c10521.

[44] G. Colombi, T. De Krom, D. Chaykina, S. Cornelius, S.W.H. Eijt, B. Dam, Influence of cation (RE=Sc, Y, Gd) and O/H anion ratio on the photochromic properties of REOxH3–2x thin films, ACS Photonics 8 (3) (2021) 709–715, http://dx.doi.org/10.1021/acsphotonics.0c01877.

[45] K. Ooya, J. Li, K. Fukui, S. Iimura, T. Nakao, K. Ogasawara, M. Sasase, H. Abe, Y. Niwa, M. Kitano, H. Hosono, Ruthenium catalysts promoted by lanthanide oxyhydrides with high hydride-ion mobility for low-temperature ammonia synthesis, Adv. Energy Mater. 11 (2021) 2003723, http://dx.doi.org/10.1002/aenm.202003723.

[46] H. Yamashita, T. Broux, Y. Kobayashi, F. Takeiri, H. Ubukata, T. Zhu, M.A. Hayward, K. Fujii, M. Yashima, K. Shitara, A. Kuwabara, T. Murakami, H. Kageyama, Chemical pressure-induced anion order–disorder transition in LnHO enabled by hydride size flexibility, J. Am. Chem. Soc. 140 (36) (2018) 11170–11173, http://dx.doi.org/10.1021/jacs.8b06187.

[47] N. Zapp, D. Sheptyakov, A. Franz, H. Kohlmann, HoHO: A paramagnetic air-resistant ionic hydride with ordered anions, Inorg. Chem. 60 (6) (2021) 3972–3979, http://dx.doi.org/10.1021/acs.inorgchem.0c03822.

[48] H. Ubukata, T. Broux, F. Takeiri, K. Shitara, H. Yamashita, A. Kuwabara, G. Kobayashi, H. Kageyama, Hydride conductivity in an anion-ordered fluorite structure LnHO with an enlarged bottleneck, Chem. Mater. 31 (18) (2019) 7360–7366, http://dx.doi.org/10.1021/acs.chemmater.9b01968.

[49] N. Zapp, D. Sheptyakov, H. Kohlmann, Computational chemistry-guided syntheses and crystal structures of the heavier lanthanide hydride oxides DyHO, ErHO, and LuHO, Crystals 11 (7) (2021) 750, http://dx.doi.org/10.3390/cryst11070750.

[50] M. Widerøe, H. Fjellvåg, T. Norby, F.W. Poulsen, R.W. Berg, NdHO, a novel oxyhydride, J. Solid State Chem. 184 (7) (2011) 1890–1894, http://dx.doi.org/10.1016/j.jssc.2011.05.025.

[51] R. Kataoka, T. Kojima, K. Tada, M. Kitta, N. Takeichi, K. Sakaki, M. Nozaki, T. Kimura, A. Kamegawa, Face-centered-cubic yttrium trihydride high-pressure phase stabilized at ambient pressures by mechanical milling, Materialia 15 (2021) 100956, http://dx.doi.org/10.1016/j.mtla.2020.100956.

[52] A. Ohmura, A. Machida, T. Watanuki, K. Aoki, S. Nakano, K. Takemura, Photochromism in yttrium hydride, Appl. Phys. Lett. 91 (2007) 151904, http://dx.doi.org/10.1063/1.2794755.

[53] N. Zapp, H. Auer, H. Kohlmann, YHO, an air-stable ionic hydride, Inorg. Chem. 58 (21) (2019) 14635–14641, http://dx.doi.org/10.1021/acs.inorgchem.9b02308.

[54] E.M. Baba, J. Montero, E. Strugovshchikov, E.Ö. Zayim, S. Karazhanov, Light-induced breathing in photochromic yttrium oxyhydrides, Phys. Rev. Mater. 4 (2020) 025201, http://dx.doi.org/10.1103/PhysRevMaterials.4.025201.

[55] F. Nafezarefi, Photochromic Properties of Rare-Earth Oxyhydrides (Ph.D. thesis), TU Delft, 2020.

[56] M. Zubkins, I. Aulika, E. Strods, V. Vibornijs, L. Bikse, A. Sarakovskis, G. Chikvaidze, J. Gabrusenoks, H. Arslan, J. Purans, Optical properties of oxygen-containing yttrium hydride thin films during and after the deposition, Vacuum 203 (2022) 111218, http://dx.doi.org/10.1016/j.vacuum.2022.111218.

[57] A. Miniotas, B. Hjörvarsson, L. Douysset, P. Nostell, Gigantic resistivity and band gap changes in GdO_yH_x thin films, Appl. Phys. Lett. 76 (15) (2000) 2056–2058, http://dx.doi.org/10.1063/1.126253.

[58] J. Montero, P. Svedlindh, L. Österlund, Photo-induced reversible modification of the Curie–Weiss temperature in paramagnetic gadolinium compounds, Solid State Commun. (2023) 115419, http://dx.doi.org/10.1016/j.ssc.2023.115419.

[59] M.V. Moro, D. Moldarev, C.C. You, E.M. Baba, S.Z. Karazhanov, M. Wolff, D. Primetzhofer, In-situ composition analysis of photochromic yttrium oxy-hydride thin films under light illumination, Sol. Energy Mater. Sol. Cells 201 (2019) 110119, http://dx.doi.org/10.1016/j.solmat.2019.110119.

[60] C.C. You, D. Moldarev, T. Mongstad, D. Primetzhofer, M. Wolff, E.S. Marstein, S.Z. Karazhanov, Enhanced photochromic response in oxygen-containing yttrium hydride thin films transformed by an oxidation process, Sol. Energy Mater. Sol. Cells 166 (2017) 185–189, http://dx.doi.org/10.1016/j.solmat.2017.03.023.

[61] J. Montero, S.Z. Karazhanov, Spectroscopic ellipsometry and microstructure characterization of photochromic oxygen-containing yttrium hydride thin films, Phys. Status Solidi (a) 215 (19) (2018) 1701039, http://dx.doi.org/10.1002/pssa.201701039.

[62] J.A. Thornton, Influence of apparatus geometry and deposition conditions on the structure and topography of thick sputtered coatings, J. Vac. Sci. Technol. 11 (4) (1974) 666–670, http://dx.doi.org/10.1116/1.1312732.

[63] A.T.M. van Gogh, D.G. Nagengast, E.S. Kooij, N.J. Koeman, J.H. Rector, R. Griessen, C.F.J. Flipse, R.J.J.G.A.M. Smeets, Structural, electrical, and optical properties of $La_{1-z}Y_zH_x$ switchable mirrors, Phys. Rev. B 63 (2001) 195105, http://dx.doi.org/10.1103/PhysRevB.63.195105.

[64] J. Montero, A. Galeckas, S.Z. Karazhanov, Photoluminescence properties of photochromic yttrium hydride films containing oxygen, Phys. Status Solidi b 255 (2018) 1800139, http://dx.doi.org/10.1002/pssb.201800139.

[65] M. Hans, T.T. Tran, S.M. Aðalsteinsson, D. Moldarev, M.V. Moro, M. Wolff, D. Primetzhofer, Photochromic mechanism and dual-phase formation in oxygen-containing rare-earth hydride thin films, Adv. Opt. Mater. 8 (2020) 2000822, http://dx.doi.org/10.1002/adom.202000822.

[66] M.H. Sørby, F. Martinsen, S.Z. Karazhanov, B.C. Hauback, E.S. Marstein, On the crystal chemistry of photochromic yttrium oxyhydride, Energies 15 (2022) 1903, http://dx.doi.org/10.3390/en15051903.

[67] G. Colombi, R. Stigter, D. Chaykina, S. Banerjee, A.P.M. Kentgens, S.W.H. Eijt, B. Dam, G.A. de Wijs, Energy, metastability, and optical properties of anion-disordered RO_xH_{3-2x} (R = Y, La) oxyhydrides: A computational study, Phys. Rev. B 105 (2022) 054208, http://dx.doi.org/10.1103/PhysRevB.105.054208.

[68] K. Kantre, M. Moro, D. Moldarev, M. Wolff, D. Primetzhofer, Synthesis and in-situ characterization of photochromic yttrium oxyhydride grown by reactive e–beam evaporation, Scr. Mater. 186 (2020) 352–356, http://dx.doi.org/10.1016/j.scriptamat.2020.05.009.

[69] D. Moldarev, D. Primetzhofer, C.C. You, S.Z. Karazhanov, J. Montero, F. Martinsen, T. Mongstad, E.S. Marstein, M. Wolff, Composition of photochromic oxygen-containing yttrium hydride films, Sol. Energy Mater. Sol. Cells 177 (2018) 66–69, http://dx.doi.org/10.1016/j.solmat.2017.05.052.

[70] C.C. You, T. Mongstad, E.S. Marstein, S.Z. Karazhanov, The dependence of structural, electrical and optical properties on the composition of photochromic yttrium oxyhydride thin films, Materialia 6 (2019) 100307, http://dx.doi.org/10.1016/j.mtla.2019.100307.

[71] American Society for Testing and Materials, Standard tables of reference, solar spectral irradiances: Direct normal and hemispherical on a 37° tilted surface, in: Annual Book of ASTM Standards, vol. 14.04, American Society for Testing and Materials, Philadelphia, PA, USA, 2008.

[72] G. Wyszecki, W. Stiles, Color Science: Concepts and Methods, Quantitative Data and Formulae, second ed., Wiley, New York, NY, USA, 2000.

[73] I. Duarte, A. Rotter, A. Malvestiti, M. Silva, The role of glass as a barrier against the transmission of ultraviolet radiation: An experimental study, Photodermatol., Photoimmunol. Photomed. 25 (4) (2009) 181–184, http://dx.doi.org/10.1111/j.1600-0781.2009.00434.x.

[74] H. Bach, N. Neuroth (Eds.), The Properties of Optical Glass, first ed., Springer Berlin, Heidelberg, 1995, http://dx.doi.org/10.1007/978-3-642-57769-7, Schott Series on Glass and Glass Ceramics.

[75] S. Li, VO_2-based Thermochromic and Nanothermochromic Materials for Energy Efficient Windows (Ph.D. thesis), Uppsala University, 2013, ISBN: 978-91-554-8801-7.

[76] B. Stjerna, E. Olsson, C.G. Granqvist, Optical and electrical properties of radio frequency sputtered tin oxide films doped with oxygen vacancies, F, Sb, or Mo, J. Appl. Phys. 76 (1994) 3797–3817, http://dx.doi.org/10.1063/1.357383.

[77] D. Ginley, H. Hosono, D. Paine, Handbook of Transparent Conductors, Springer US, 2010, URL https://books.google.es/books?id=K0qjBlrAGYsC.

[78] J.I. Pankove, Optical Processes in Semiconductors, Dover, 1975.

[79] C.C. You, T. Mongstad, J.P. Maehlen, S. Karazhanov, Engineering of the band gap and optical properties of thin films of yttrium hydride, Appl. Phys. Lett. 105 (3) (2014) http://dx.doi.org/10.1063/1.4891175.

[80] W. Lau, Double duty, 2012, The Journal of the American Institute of Architects. URL https://www.architectmagazine.com/technology/products/double-duty_o.

[81] Energy performance ratings for windows, doors, and skylights, 2023, https://www.energy.gov/energysaver/energy-performance-ratings-windows-doors-and-skylights. (Accessed 17 December 2023).

[82] C.G. Granqvist, Transparent conductors as solar energy materials: A panoramic review, Sol. Energy Mater. Sol. Cells 91 (17) (2007) 1529–1598, http://dx.doi.org/10.1016/j.solmat.2007.04.031.

[83] C.M. Garnett, Colours in metal glasses and in metallic films, Philos. Trans. R. Soc. Lond. A Math. Phys. Eng. Sci. 203 (359–371) (1904) 385–420.

[84] J.C.M. Garnett, Colours in metal glasses, in metallic films, and in metallic solutions. II, Philos. Trans. R. Soc. Lond. A Math. Phys. Eng. Sci. 205 (387–401) (1906) 237–288.

[85] D. Moldarev, M. Wolff, E. Baba, M. Moro, C. You, D. Primetzhofer, S. Karazhanov, Photochromic properties of yttrium oxyhydride thin films: Surface versus bulk effect, Materialia 11 (2020) 100706, http://dx.doi.org/10.1016/j.mtla.2020.100706.

[86] S. Kazi, D. Moldarev, M. Moro, D. Primetzhofer, M. Wolff, Correlating photoconductivity and optical properties in oxygen-containing yttrium hydride thin films, Phys. Status Solidi RRL 17 (2023) 2200435, http://dx.doi.org/10.1002/pssr.202200435.

[87] J. Montero, F.A. Martinsen, M. García-Tecedor, S.Z. Karazhanov, D. Maestre, B. Hauback, E.S. Marstein, Photochromic mechanism in oxygen-containing yttrium hydride thin films: An optical perspective, Phys. Rev. B 95 (2017) 201301, http://dx.doi.org/10.1103/PhysRevB.95.201301.

[88] Y. Komatsu, R. Shimizu, R. Sato, M. Wilde, K. Nishio, T. Katase, D. Matsumura, H. Saitoh, M. Miyauchi, J.R. Adelman, et al., Repeatable photoinduced insulator-to-metal transition in yttrium oxyhydride epitaxial thin films, Chem. Mater. 34 (8) (2022) 3616–3623, http://dx.doi.org/10.1021/acs.chemmater.1c03450.

[89] Z. Wu, T. de Krom, G. Colombi, D. Chaykina, G. van Hattem, H. Schut, M. Dickmann, W. Egger, C. Hugenschmidt, E. Brück, B. Dam, S.W.H. Eijt, Formation of vacancies and metallic-like domains in photochromic rare-earth oxyhydride thin films studied by in-situ illumination positron annihilation spectroscopy, Phys. Rev. Mater. 6 (2022) 065201, http://dx.doi.org/10.1103/PhysRevMaterials.6.065201.

[90] M.P. Plokker, S.W.H. Eijt, F. Naziris, H. Schut, F. Nafezarefi, H. Schreuders, S. Cornelius, B. Dam, Electronic structure and vacancy formation in photochromic yttrium oxy-hydride thin films studied by positron annihilation, Sol. Energy Mater. Sol. Cells 177 (2018) 97–105, http://dx.doi.org/10.1016/j.solmat.2017.03.011.

[91] G. Colombi, B. Boshuizen, D. Chaykina, L. Hsu, H. Schreuders, T.J. Savenije, B. Dam, Large polaron conduction, photoconductivity, and photochromism in GdO_xH_{3-2x} oxyhydride thin films, Adv. Opt. Mater. 11 (2023) 2202660, http://dx.doi.org/10.1002/adom.202202660.

[92] D. Chaykina, I. Usman, G. Colombi, H. Schreuders, B. Tyburska-Pueschel, Z. Wu, S.W.H. Eijt, L.J. Bannenberg, G.A. de Wijs, B. Dam, Aliovalent calcium doping of yttrium oxyhydride thin films and implications for photochromism, J. Phys. Chem. C 126 (34) (2022) 14742–14749, http://dx.doi.org/10.1021/acs.jpcc.2c04456.

[93] J.P. Maehlen, T.T. Mongstad, C.C. You, S. Karazhanov, Lattice contraction in photochromic yttrium hydride, J. Alloys Compd. 580 (2013) S119–S121, http://dx.doi.org/10.1016/j.jallcom.2013.03.151.

[94] S. Aðalsteinsson, M.V. Moro, D. Moldarev, S. Droulias, M. Wolff, D. Primetzhofer, Correlating chemical composition and optical properties of photochromic rare-earth oxyhydrides using ion beam analysis, Nucl. Instrum. Methods Phys. Res. B 485 (2020) 36–40, http://dx.doi.org/10.1016/j.nimb.2020.09.016.

[95] E.M. Baba, J. Montero, D. Moldarev, M.V. Moro, M. Wolff, D. Primetzhofer, S. Sartori, E. Zayim, S. Karazhanov, Preferential orientation of photochromic gadolinium oxyhydride films, Molecules 25 (2020) 3181, http://dx.doi.org/10.3390/molecules25143181.

[96] S. Banerjee, D. Chaykina, R. Stigter, G. Colombi, S.W. Eijt, B. Dam, G.A. de Wijs, A.P. Kentgens, Exploring multi-anion chemistry in yttrium oxyhydrides: Solid-state NMR studies and DFT calculations, J. Phys. Chem. C 127 (29) (2023) 14303–14316, http://dx.doi.org/10.1021/acs.jpcc.3c02680.

[97] T. Mongstad, C. Platzer-Björkman, J.P. Mæhlen, B.C. Hauback, S.Z. Karazhanov, F. Cousin, Surface oxide on thin films of yttrium hydride studied by neutron reflectometry, Appl. Phys. Lett. 100 (19) (2012) 191604, http://dx.doi.org/10.1063/1.4714517.

[98] R.D. Shannon, Revised effective ionic radii and systematic studies of interatomic distances in halides and chalcogenides, Acta Cryst. A 32 (5) (1976) 751–767, http://dx.doi.org/10.1107/S0567739476001551.

[99] C.C. You, S.Z. Karazhanov, Effect of temperature and illumination conditions on the photochromic performance of yttrium oxyhydride thin films, J. Appl. Phys. 128 (1) (2020) 013106, http://dx.doi.org/10.1063/5.0010132.

[100] F. Nafezarefi, S. Cornelius, J. Nijskens, H. Schreuders, B. Dam, Effect of the addition of zirconium on the photochromic properties of yttrium oxy-hydride, Sol. Energy Mater. Sol. Cells 200 (2019) 109923, http://dx.doi.org/10.1016/j.solmat.2019.109923.

[101] R.S. Hallaråker, Temperature- and Irradiation-Dependent Properties of Photochromic Thin Films Of YHx:O (Master's thesis), Norwegian University of Life Sciences (NMBU), 2018, http://hdl.handle.net/11250/2570466.

[102] E.M. Baba, P.M. Weiser, E. Zayim, S. Karazhanov, Temperature-dependent photochromic performance of yttrium oxyhydride thin films, Phys. Status Solidi RRL 15 (2021) 2000459, http://dx.doi.org/10.1002/pssr.202000459.

[103] R.S. Ulrich, View through a window may influence recovery from surgery, Science 224 (4647) (1984) 420–421, http://dx.doi.org/10.1126/science.6143402.

[104] L. Lottrup, U. Stigsdotter, H. Meilby, A. Claudi, The workplace window view: A determinant of office workers' work ability and job satisfaction, Landsc. Res. 40 (2015) 57–75, http://dx.doi.org/10.1080/01426397.2013.829806.

[105] R. Baloch, C. Nichole Maesano, J. Christoffersen, C. Mandin, E. Csobod, E. de Oliveira Fernandes, I. Annesi-Maesano, on behalf of the SINPHONIE Consortium, Daylight and school performance in European schoolchildren, Int. J. Environ. Res. Public Health 18 (2021) 258, http://dx.doi.org/10.3390/ijerph18010258.

[106] N.E. Klepeis, W.C. Nelson, W.R. Ott, J.P. Robinson, A.M. Tsang, P. Switzer, J.V. Behar, S.C. Hern, W.H. Engelmann, The national human activity pattern survey (NHAPS): A resource for assessing exposure to environmental pollutants, J. Expo. Anal. Environ. Epidemiol. 11 (3) (2001) 231–252, http://dx.doi.org/10.1038/sj.jea.7500165.

[107] V. Maiorov, Optical properties of thermotropic hydrogels (a review), Opt. Spectrosc. 128 (2020) 367–386.

[108] S. Arbab, B. Szybinska Matusiak, F.A. Martinsen, B.C. Hauback, The impact of advanced glazing on colour perception, J. Int. Colour Assoc. 17 (2017) 50–68.

[109] S. Arbab, B. Szybinska Matusiak, A. Klökner, Colour shift of interior surfaces with advanced glazings, J. Int. Colour Assoc. 21 (2018) 10–35.

[110] J. Montero, Y.-X. Ji, C.G. Granqvist, G.A. Niklasson, Thermochromic light scattering from particulate VO_2 layers, J. Appl. Phys. 119 (2016) 085302, http://dx.doi.org/10.1063/1.4942211.

[111] C. Guillén, J. Montero, J. Herrero, Transparent and conductive electrodes combining AZO and ATO thin films for enhanced light scattering and electrical performance, Appl. Surf. Sci. 264 (2013) 448–452, http://dx.doi.org/10.1016/j.apsusc.2012.10.042.

[112] P. Nitz, H. Hartwig, Solar control with thermotropic layers, Sol. Energy 79 (6) (2005) 573–582, http://dx.doi.org/10.1016/j.solener.2004.12.009, Polymeric Materials for Solar Energy Applications.

[113] X.-H. Li, C. Liu, S.-P. Feng, N.X. Fang, Broadband light management with thermochromic hydrogel microparticles for smart windows, Joule 3 (1) (2019) 290–302, http://dx.doi.org/10.1016/j.joule.2018.10.019.

[114] D. Moldarev, M.V. Moro, C.C. You, E.M. Baba, S.Z. Karazhanov, M. Wolff, D. Primetzhofer, Yttrium oxyhydrides for photochromic applications: Correlating composition and optical response, Phys. Rev. Mater. 2 (2018) 115203, http://dx.doi.org/10.1103/PhysRevMaterials.2.115203.

[115] D. Moldarev, L. Stolz, M.V. Moro, S.M. Aðalsteinsson, I.-A. Chioar, S.Z. Karazhanov, D. Primetzhofer, M. Wolff, Environmental dependence of the photochromic effect of oxygen-containing rare-earth metal hydrides, J. Appl. Phys. 129 (15) (2021) http://dx.doi.org/10.1063/5.0041487.

[116] J. Chen, In-Situ Study of the Chemical Composition of Photochromic Yttrium Oxy-Hydrides Thin Films (Master's thesis), Uppsala university, 2019, urn:nbn:se:uu:diva-389390.

[117] K. Hollands, J. Wright, C. Granqvist, Glazings and coatings, in: J.M. Gordon (Ed.), Solar Energy: The State of the Art, Routledge, London, UK, 2013, pp. 29–107, http://dx.doi.org/10.4324/9781315074412.

[118] C. Bechinger, G. Oefinger, S. Herminghaus, P. Leiderer, On the fundamental role of oxygen for the photochromic effect of WO_3, J. Appl. Phys. 73 (7) (1993) 4527–4533, http://dx.doi.org/10.1063/1.354370.

[119] D. Vollath, Nanomaterials: An Introduction to Synthesis, Properties and Applications, first ed., Wiley, 2013.

[120] M.V. Santos, H.S. Barud, M.A. Alencar, M. Nalin, S.H. Toma, K. Araki, A.V. Benedetti, I.O. Maciel, B. Fragneaud, C. Legnani, et al., Self-supported smart bacterial nanocellulose–phosphotungstic acid nanocomposites for photochromic applications, Front. Mater. 8 (2021) 668835, http://dx.doi.org/10.3389/fmats.2021.668835.

[121] M.V. Moro, S.M. Aðalsteinsson, T.T. Tran, D. Moldarev, A. Samanta, M. Wolff, D. Primetzhofer, Photochromic response of encapsulated oxygen-containing yttrium hydride thin films, Phys. Status Solidi (RRL)–Rapid Res. Lett. 15 (6) (2021) 2000608, http://dx.doi.org/10.1002/pssr.202000608.

[122] W.M. Haynes (Ed.), CRC Handbook of Chemistry and Physics, ninety seventh ed., CRC Press, Boca Raton, 2016, p. 2670, http://dx.doi.org/10.1201/9781315380476.

[123] J. Cui, M. Kramer, L. Zhou, F. Liu, A. Gabay, G. Hadjipanayis, B. Balasubramanian, D. Sellmyer, Current progress and future challenges in rare-Earth-free permanent magnets, Acta Mater. 158 (2018) 118–137, http://dx.doi.org/10.1016/j.actamat.2018.07.049.

[124] R. Ganguli, D.R. Cook, Rare Earths: A review of the landscape, MRS Energy Sustain. 5 (1) (2018) 6, http://dx.doi.org/10.1557/mre.2018.7.

[125] P. Alves Dias, S. Bobba, S. Carrara, B. Plazzotta, et al., The Role of Rare Earth Elements in Wind Energy and Electric Mobility – An Analysis of Future Supply/Demand Balances, Tech. Rep., European Commission, Joint Research Centre, 2020, https://data.europa.eu/doi/10.2760/303258.

[126] Y. Kobayashi, O. Hernandez, C. Tassel, H. Kageyama, New chemistry of transition metal oxyhydrides, Sci. Technol. Adv. Mate. 18 (1) (2017) 905–918, http://dx.doi.org/10.1080/14686996.2017.1394776.